



CERN-PH-EP/2012-316

2018/11/06

CMS-SUS-11-028

Search for supersymmetry in final states with a single lepton, b-quark jets, and missing transverse energy in proton-proton collisions at $\sqrt{s} = 7 \text{ TeV}$

The CMS Collaboration^{*}

Abstract

A search motivated by supersymmetric models with light top squarks is presented using proton-proton collision data recorded with the CMS detector at a center-of-mass energy of $\sqrt{s} = 7 \text{ TeV}$ during 2011, corresponding to an integrated luminosity of 4.98 fb^{-1} . The analysis is based on final states with a single lepton, b-quark jets, and missing transverse energy. Standard model yields are predicted from data using two different approaches. The observed event numbers are found to be compatible with these predictions. Results are interpreted in the context of the constrained minimal supersymmetric standard model and of a simplified model with four top quarks in the final state.

Submitted to Physical Review D

1 Introduction

In this paper we describe a search for supersymmetry (SUSY) in final states with a single electron or muon, multiple jets, including some identified as originating from b quarks (b jets), and missing transverse energy. The search is based on the full set of data recorded with the Compact Muon Solenoid (CMS) experiment in proton-proton collisions at a center-of-mass energy of $\sqrt{s} = 7\text{ TeV}$ during 2011, which corresponds to an integrated luminosity of $4.98 \pm 0.11\text{ fb}^{-1}$.

The search for new physics phenomena in events with third-generation quarks at the Large Hadron Collider (LHC) is motivated by various extensions [1–5] of the standard model (SM). Among these, supersymmetric models are regarded as attractive, because they can resolve the hierarchy problem and may permit the unification of the electroweak and strong interactions [6–10].

Supersymmetry predicts that for each particle in the SM there exists a partner particle, often referred to as a sparticle, with identical gauge quantum numbers but with a spin that differs by 1/2. Assuming R parity conservation [11], sparticles are produced in pairs, and their decay chains terminate with the lightest supersymmetric particle (LSP). In some scenarios the LSP is the lightest neutralino ($\tilde{\chi}_1^0$), a heavy, electrically neutral, weakly interacting particle, which is a viable dark-matter candidate. In these scenarios, SUSY events are characterized by missing transverse energy in the final state.

In several SUSY scenarios, particularly motivated by naturalness of the spectrum [12, 13], top (\tilde{t}) or bottom (\tilde{b}) squarks may be copiously produced at the LHC. This may happen by direct squark production, e.g., $\text{pp} \rightarrow \tilde{t}\tilde{t}^* \rightarrow t\bar{t}\tilde{\chi}_1^0\tilde{\chi}_1^0$. If the mass of the gluino (\tilde{g}) is larger than the masses of the third-generation squarks, but lighter than the squarks of the first two generations, the gluino may dominantly decay into the third-generation squarks, e.g., $\tilde{g} \rightarrow t\bar{t}^* \rightarrow t\bar{t}\tilde{\chi}_1^0$. Hence gluino pair production can lead to events containing four third-generation quarks, resulting in an excess of events with large b-jet multiplicities, which is exploited by dedicated analyses [14–20].

The decay chains of the strongly interacting particles predicted by these models result in a high level of hadronic activity, characterized by a large number of high-energy jets. In addition, isolated leptons may originate from leptonically decaying top quarks and two- or three-body decays of neutralinos and charginos.

The search is performed in signal regions defined using the scalar sum of the jet transverse momenta H_T , the missing transverse energy \cancel{E}_T , and the b-jet multiplicity. The dominant SM background processes contributing to the search topology are top-quark pair ($t\bar{t}$) production and inclusive W-boson production in association with energetic jets (W+jets). Smaller contributions are due to single-top production, QCD multijet events (QCD), and Drell-Yan (DY) production and decay to lepton pairs in which one lepton goes undetected. While simulation provides a good description of these contributions, more reliable estimates of the backgrounds can be obtained from data.

To evaluate the SM background, two complementary data-based approaches are used. In the first approach, templates for the \cancel{E}_T spectra in $W^- + \text{jets}$, $W^+ + \text{jets}$, and $t\bar{t}$ production are extracted from the inclusive single-lepton sample by a simultaneous fit to the 0, 1, and ≥ 2 b-jet subsamples. This fit involves the convolution of a model for the true \cancel{E}_T distribution with detector effects determined using data in control regions at low H_T . Predictions in several signal regions defined by different selections on H_T , \cancel{E}_T , and for 0, 1, and ≥ 2 identified b jets are obtained by applying the templates at high values of H_T after normalization in background-dominated regions at low \cancel{E}_T . The second approach, a factorization method, predicts the expected number

of background events in a subsample with high H_T and Y_{MET} , where $Y_{\text{MET}} = \cancel{E}_T / \sqrt{H_T}$ is an approximate measure of the \cancel{E}_T significance. Since H_T and Y_{MET} are only weakly correlated, the estimate can be obtained using a factorization approach based on three background-dominated control regions and can be calculated independently for different b-jet multiplicities. Therefore, it naturally provides an estimate for a selection with ≥ 3 identified b-jets, yielding a better signal-to-noise ratio for SUSY models with many (at least 3) b jets. The use of a background estimation technique based on data reduces the uncertainty on the prediction by more than a factor of two. While both methods use the H_T and \cancel{E}_T variables, they have only a small overlap in their control and signal regions, both in the SM and in the signal scenarios, and are therefore complementary.

The analyses presented here are not limited to a particular theory. However, the constrained minimal supersymmetric extension of the standard model (CMSSM) [21, 22] is chosen as a benchmark to illustrate the sensitivity of this search for new-physics processes. The template method in the 0, 1, and ≥ 2 b-jet subsamples shows the best sensitivity in the parameter plane of this model. A scenario involving four top quarks in the final state is used as the second benchmark. It is implemented as a scenario in the context of simplified model spectra (SMS) [23–25]. The factorization method with the ≥ 3 b-jet subsample is best suited for this topology.

A brief description of the CMS detector is given in Section 2. The datasets and simulated event samples used in this search are discussed in Section 3. In Section 4 the preselection of physics objects and events is outlined. The \cancel{E}_T template and factorization methods are described in Sections 5 and 6, respectively. Results are presented in Section 7 and interpreted in Section 8. Finally a summary is given in Section 9.

2 The CMS Detector

The CMS detector is a multipurpose apparatus designed to allow the study of high transverse momentum (p_T) processes in proton-proton collisions, as well as a broad range of phenomena in heavy-ion collisions. The CMS coordinate system is defined with the origin at the center of the detector and the z axis along the counterclockwise beam direction, with ϕ the azimuthal angle (measured in radians), θ the polar angle, and $\eta = -\ln[\tan(\theta/2)]$ the pseudorapidity.

The central feature of the detector is a superconducting solenoid, 13 m in length and 6 m in diameter, which provides an axial magnetic field of 3.8 T. Within the magnet are the silicon pixel and strip detectors for charged-particle tracking, a lead-tungstate crystal electromagnetic calorimeter for measurements of photons, electrons, and the electromagnetic component of jets, and a hadron calorimeter, constructed from scintillating tiles and brass absorbers, for jet energy measurements. The tracker covers the region $|\eta| < 2.5$ and the calorimeters $|\eta| < 3.0$. A quartz-steel forward calorimeter using Cherenkov radiation extends the coverage to $|\eta| \leq 5$. The detector is nearly hermetic, allowing for energy-balance measurements in the plane transverse to the beam direction. Outside the magnet is the muon system, comprising drift-tube, cathode-strip, and resistive-plate detectors, all interleaved with steel absorbers acting as a magnetic flux return. A detailed description of the CMS detector can be found elsewhere [26].

3 Event Samples

The events are selected with triggers requiring the presence of a muon or electron with large transverse momentum p_T in association with significant hadronic activity, quantified by H_T^{trigger} , the value of H_T calculated at the trigger level. In the second part of the year a requirement on

H_T^{trigger} , the magnitude of the vectorial sum of the transverse momenta of jets, was added.

In order not to exceed the maximum possible rate of data acquisition and processing, trigger thresholds were raised with increasing LHC luminosity, resulting in a threshold for the muon transverse momentum p_T from 8 GeV to 15 GeV, and for electrons from 10 GeV to 15 GeV. The requirement on the hadronic activity was raised from $H_T^{\text{trigger}} > 200$ GeV to $H_T^{\text{trigger}} > 300$ GeV in the muon and to $H_T^{\text{trigger}} > 250$ GeV in the electron channel. The requirement on H_T^{trigger} was introduced with a threshold of 20 GeV that was later raised to 40 GeV.

Simulated event samples are produced using different event generators and the GEANT4 package [27] for detector simulation, except for the scans of CMSSM and SMS parameter space discussed below. The production and decay of $t\bar{t}$ pairs or vector bosons in association with energetic jets are generated using the MADGRAPH 5.1.1 [28] generator. The produced parton events are then passed to the PYTHIA 6.4.24 [29] program with tune Z2 [30] for simulating parton showers, multiple interactions, and fragmentation processes. The decay of τ leptons is simulated using the TAUOLA 27.121.5 [31] program. The production and decay of single top quarks and antiquarks are simulated with the POWHEG 301 [32, 33] and TAUOLA generators interfaced to PYTHIA. Multijet QCD production is simulated with PYTHIA.

Mass spectra and branching fractions of SUSY particles are calculated at the electroweak scale using the renormalization equations implemented in the SOFTSUSY package [34], interfaced to PYTHIA. Two low-mass scenarios [35] are used as CMSSM benchmark points to illustrate possible yields: the first one is referred to as LM6 ($m_0 = 85$ GeV, $m_{1/2} = 400$ GeV, $A_0 = 0$ GeV, $\tan \beta = 10$, $\mu > 0$), and the second one as LM8 ($m_0 = 500$ GeV, $m_{1/2} = 300$ GeV, $A_0 = -300$ GeV, $\tan \beta = 10$, $\mu > 0$). In other event topologies these points have been experimentally excluded [14, 15, 36].

A scan in the CMSSM parameter space is performed for a fixed set of parameters: A_0 , $\tan \beta$, and sign μ , where a grid in the m_0 - $m_{1/2}$ plane is defined by variation of m_0 and $m_{1/2}$ in steps of 20 GeV. For each point, 10 000 pp events are generated.

In addition, the results are interpreted in the context of the simplified model shown in Fig. 1. It contains the pair production of gluinos, which subsequently decay with branching fraction $\mathcal{B}(\tilde{g} \rightarrow t\bar{t} + \tilde{\chi}_1^0) = 1$. For each point on a 25 GeV \times 25 GeV grid in the parameter plane of the gluino and $\tilde{\chi}_1^0$ masses, 50 000 events are simulated. The events in the CMSSM and SMS scans are generated using a fast detector simulation [37] rather than the GEANT4 package.

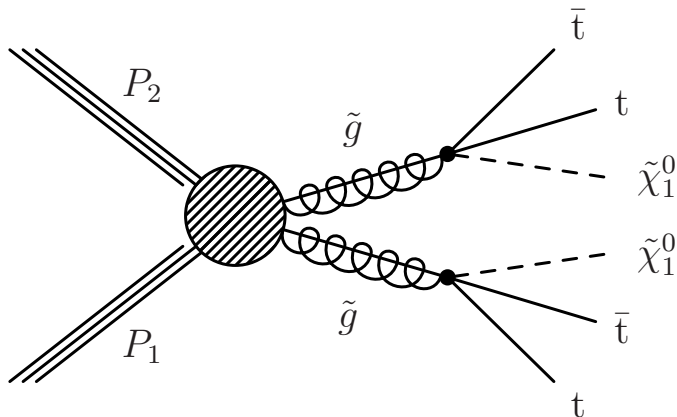


Figure 1: Diagram for the simplified model used in this paper.

4 Event Selection

The primary vertex must satisfy a set of quality requirements, including the restriction that the longitudinal and transverse distances of the primary vertex from the nominal interaction point be less than 24 cm and 2 cm, respectively.

Muon candidates [38] are required to have $p_T(\mu) > 20 \text{ GeV}$ and $|\eta| < 2.1$. The reconstructed track of a muon candidate must have an impact parameter less than 0.02 cm in the transverse plane and less than 1.0 cm along the beam axis, where the impact parameter is the distance of the track trajectory to the primary vertex at the point of closest approach in the transverse plane. To suppress background contributions from muons originating from heavy-flavor quark decays, the muon is required to be isolated within a cone of size $\Delta R = 0.3$, with $\Delta R = \sqrt{(\Delta\eta)^2 + (\Delta\phi)^2}$. The relative combined isolation of the muon is defined as $I_{\text{rel}}^{\text{comb}} = \sum_{\Delta R < 0.3} (E_T + p_T)/p_T(\mu)$, where the sum is over the transverse energy E_T (as measured in the electromagnetic and hadron calorimeters) and the transverse momentum p_T (as measured in the silicon tracker) of all reconstructed objects within this cone, excluding the track itself. Muons are required to satisfy $I_{\text{rel}}^{\text{comb}} < 0.1$.

Electron candidates [39] are restricted to $p_T > 20 \text{ GeV}$ and $|\eta| < 2.4$, excluding the barrel-endcap transition region ($1.44 < |\eta| < 1.57$). The reconstructed track of an electron candidate must fulfill the same impact parameter requirements as the muon tracks described above, as well as a set of quality and photon-conversion rejection criteria. The relative combined isolation variable, similar to that defined in the muon case, must satisfy $I_{\text{rel}}^{\text{comb}} < 0.07$ in the barrel region and $I_{\text{rel}}^{\text{comb}} < 0.06$ in the endcaps.

Exactly one selected muon or electron is required to be present in the event. Events with a second lepton passing looser selection criteria are rejected.

The reconstruction of jets is based on the CMS particle-flow algorithm [40], which identifies and reconstructs charged hadrons, electrons, muons, photons, and neutral hadrons. Extra energy clustered into jets due to additional, simultaneous pp collisions (“pileup”) is taken into account with an event-by-event correction to the jet four-vectors [41]. Therefore, the pileup does not have a strong influence on this analysis. Jets are reconstructed from particle-flow candidates using the anti- k_T clustering algorithm [42] with distance parameter 0.5. Corrections are applied on the raw jet energy to obtain a uniform response across the detector in η and an absolute calibrated response in p_T [43]. Each event is required to contain at least three jets with $p_T > 40 \text{ GeV}$ and $|\eta| < 2.4$ that are spatially separated from a selected muon or electron by $\Delta R > 0.3$ and that satisfy quality criteria in order to suppress noise and spurious calorimeter energy deposits.

The identification of b jets (“b-tagging”) [44] is performed with two complementary approaches. In the first approach, the distance between a reconstructed secondary vertex with two or more associated tracks and the primary interaction point, normalized to its uncertainty, is used (simple secondary-vertex algorithm). This algorithm has been shown to be particularly robust against variation in the running conditions and is used for the template method. In the second approach, jets are tagged as b jets if they have at least two tracks with an impact parameter divided by its uncertainty that is greater than 3.3 (track counting algorithm). This algorithm is highly efficient at high jet p_T and is used for the factorization method. At the chosen operating points, the efficiency to tag b jets is approximately 60 to 70%, with a misidentification rate for light-quark- or gluon-initiated jets of a few percent. The b-tagging efficiencies and mistagging rates (the efficiency of tagging a c-quark jet, light-quark jet, or gluon jet as b jet) have been measured up to jet p_T of 670 GeV for both methods.

The missing transverse energy \cancel{E}_T is reconstructed as the magnitude of the sum of the transverse momentum vectors of all particle-flow objects with $|\eta| < 4.7$. The quantity H_T , a measure of the total hadronic activity, is calculated as the sum of the transverse momenta of all jets passing the selection. Since SUSY models predict events with large hadronic activity and large amounts of missing energy, the final search regions for the two methods are defined by stringent selections on H_T and \cancel{E}_T and by the number of identified b jets, as described in the following two sections.

These selection steps define a sample that matches the trigger requirements and the expected characteristics of signal events, while retaining a sufficient number of events to allow evaluation of the background.

The trigger and lepton-reconstruction efficiencies are measured from data. The determination of the trigger efficiency is performed separately for each component of the trigger: the leptonic, the H_T^{trigger} , and the $\cancel{E}_T^{\text{trigger}}$ selection. The leptonic trigger selection is found to be 97–98% efficient after the offline requirements, for all running periods. The H_T^{trigger} requirement, and the $\cancel{E}_T^{\text{trigger}} > 20 \text{ GeV}$ trigger requirement used for the first part of the running period, are both more than 99% efficient. The $\cancel{E}_T^{\text{trigger}} > 40 \text{ GeV}$ requirement used for latter part of the running period is around 80% efficient for \cancel{E}_T values of 60 GeV, becoming fully efficient for $\cancel{E}_T > 80 \text{ GeV}$.

The offline lepton reconstruction, identification, and isolation efficiencies are measured with a “tag-and-probe” method [45], using dileptons with invariant mass close to the Z peak. The measured efficiencies have been compared to simulation as a function of p_T , η , and the number of reconstructed primary vertices and jets in the event. The total lepton efficiency in data is described by simulation to a relative accuracy within 3%.

5 The \cancel{E}_T Template Method

For the \cancel{E}_T template method, we consider overlapping signal regions with lower boundaries in H_T at 750 GeV or 1000 GeV, and with lower boundaries in \cancel{E}_T at 250 GeV, 350 GeV, and 450 GeV as shown in Fig. 2. All signal regions are restricted to $H_T < 2.5 \text{ TeV}$ and $\cancel{E}_T < 2 \text{ TeV}$ since the uncertainties for the prediction increase for very high values of these variables while the additional signal yield is small. In the \cancel{E}_T template approach, parameters of a model for the true \cancel{E}_T spectrum are obtained from a fit to a control region in data defined by $350 < H_T < 700 \text{ GeV}$ and $100 < \cancel{E}_T < 400 \text{ GeV}$. Separate \cancel{E}_T models are used for the dominant background processes: $W^- + \text{jets}$, $W^+ + \text{jets}$, and $t\bar{t}$ production. The absolute scale for the prediction is obtained from a normalization region defined by $750 < H_T < 2500 \text{ GeV}$ and $100 < \cancel{E}_T < 250 \text{ GeV}$. Figure 3 shows the difference in the \cancel{E}_T distributions of the simulated background and the two reference SUSY signals LM6 and LM8 in the muon channel at low and high H_T . The \cancel{E}_T shape used for the predictions in the signal regions is obtained from data and does not depend on the simulated distribution. Control and normalization regions have been chosen to provide a sufficiently large range in \cancel{E}_T for the fit and to limit signal contamination. The method provides background estimates for events with 0, 1, and ≥ 2 identified b jets in a natural way.

5.1 Discrimination of W from $t\bar{t}$ using b-jet identification

In order to gain sensitivity to the differences between the \cancel{E}_T shapes in $W + \text{jets}$ and $t\bar{t}$ events, we divide the preselected sample into three bins of b-jet multiplicity, corresponding to different relative proportions of $t\bar{t}$ and $W + \text{jets}$ events. Simulation predicts the 0 b-tag bin to contain 76% $W + \text{jets}$ and 19% $t\bar{t}$ events, while the ≥ 2 b-tag bin is dominated by $t\bar{t}$ events (3% $W + \text{jets}$ versus 90% $t\bar{t}$ events). The 1 b-tag bin shows intermediate values (20% $W + \text{jets}$ versus 72% $t\bar{t}$ events).

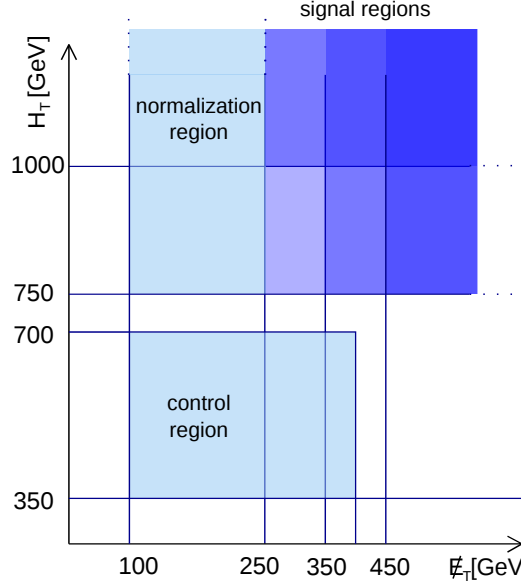


Figure 2: Graphical representation of the different regions in H_T vs. \cancel{E}_T space used in the \cancel{E}_T method.

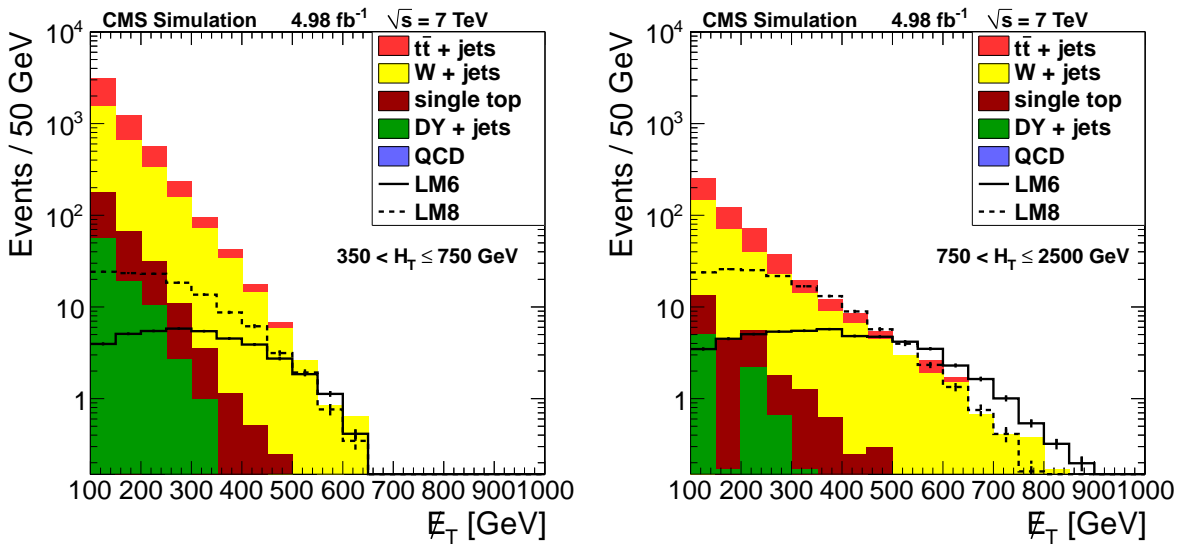


Figure 3: Distribution of \cancel{E}_T in the muon channel: simulation of backgrounds and two reference SUSY signals (LM6 and LM8) for (left) $350 < H_T < 750 \text{ GeV}$ and (right) $750 < H_T < 2500 \text{ GeV}$. No requirements are imposed on the number of b jets.

The ratio of W^+ +jets to W^- +jets in the sample is predicted to be approximately 3.

The relative fraction of W +jets and $t\bar{t}$ events is estimated from data using a template fit for the event fractions in the three b-jet multiplicity bins. The templates are extracted from simulation and corrected for the measured differences in b-quark and light-flavor tagging probabilities between data and simulation.

The evolution of the ratios in the 0 b-tag and 1 b-tag bins as a function of H_T is obtained by dividing the H_T distributions of W +jets and $t\bar{t}$ events, weighted according to the global W +jets-to- $t\bar{t}$ ratio in these bins obtained as described above. The H_T distribution for $t\bar{t}$ events is extracted from the ≥ 2 b-tag bin. The corresponding shape for W +jets events is obtained by subtracting the $t\bar{t}$ contribution from the 0 b-tag bin according to the measured $t\bar{t}$ fraction in this bin. The ratios measured in the data exhibit no significant trend with H_T .

5.2 The \cancel{E}_T model

In the region well above the W mass, namely $\cancel{E}_T > 100$ GeV, the true \cancel{E}_T spectra of the leading backgrounds are characterized by nearly exponential falling shapes. Small differences can be observed as functions of the production process, W polarization, and rapidity distributions. The functional form $x \exp(-\alpha x^\beta)$ with $\beta = 0.5$ provides a satisfactory parametrization of the inclusive distributions within each category ($t\bar{t}$, W^+ +jets, and W^- +jets). The shapes for W^+ +jets and W^- +jets are distinguished from each other using the lepton charge, and separate models are used for the two lepton flavors in order to take into account differences in the acceptance.

The selection in H_T leads to a clear bias in the \cancel{E}_T distribution due to the correlation between the transverse momentum of the W boson and the hadronic activity balancing this momentum. The shape of the ratio of the \cancel{E}_T spectrum after a selection in H_T to the inclusive spectrum can be well described by error functions, $\text{erf}(x; b, c)$, with two free parameters: the \cancel{E}_T value where the ratio reaches 50%, denoted b , and the width, denoted c . The evolution of the parameters b and c can be approximated well by linear functions of H_T : $b(H_T) = b_0 + b_1 H_T$ and $c(H_T) = c_0 + c_1 H_T$. The values for b_0 , b_1 , c_0 , and c_1 are obtained from simulation and verified with data. A second-order polynomial is used as an alternative parametrization in order to assign a systematic uncertainty to the residual non-linearity.

The full \cancel{E}_T model for a final-state category (W^+ +jets, W^- +jets, or $t\bar{t}$) in a single H_T bin i with lower and upper limits $H_{T,i}$ and $H_{T,i+1}$ has the form

$$\begin{aligned} \mathcal{M}_i(x) \sim & x \exp(-\alpha x^{0.5}) \times \\ & (1 + \text{erf}(x; b_0 + b_1 H_{T,i}, c_0 + c_1 H_{T,i})) \times \\ & (1 - \text{erf}(x; b_0 + b_1 H_{T,i+1}, c_0 + c_1 H_{T,i+1})). \end{aligned} \quad (1)$$

The categories are combined with the weights described above. The results of fits to the parameter α in bins of H_T after constraining the parameters b and c to linear functions are shown in Fig. 4. They show no significant trend, and a single value is used for each category in the final estimate.

As the model for the true \cancel{E}_T spectrum is empirical, systematic uncertainties due to the choice of the model have been evaluated by varying the parameter β in the exponential form; the parameters b and c of the error function; and the evolution of α , b , and c with H_T . Details are given in Section 5.5.

In order to describe the data, the model for the true \cancel{E}_T distribution needs to be modified

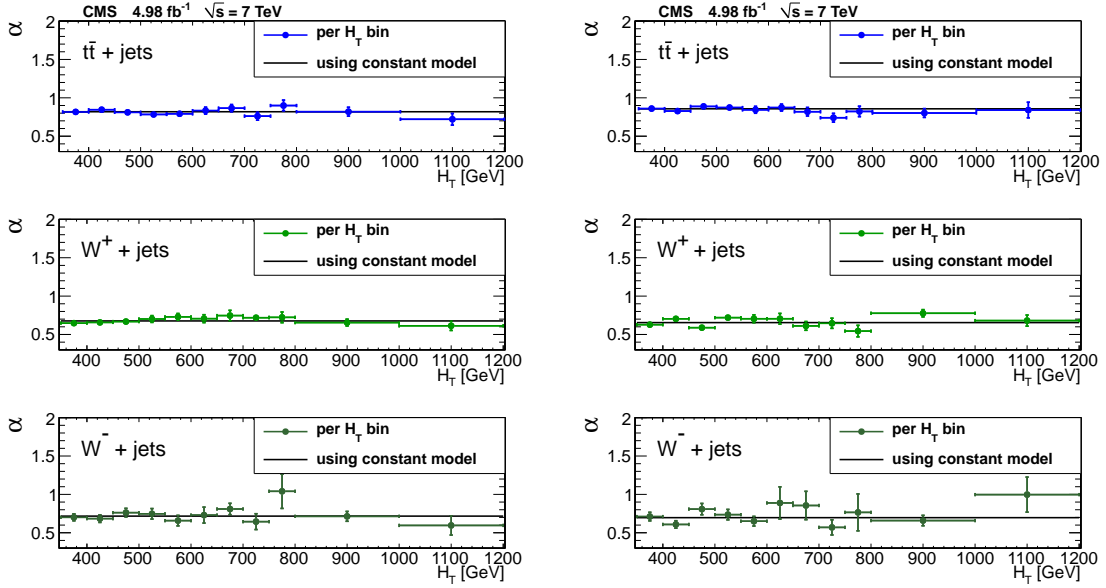


Figure 4: The fitted parameter α as a function of H_T for three subsamples of the (left) muon and (right) electron channel: from top to bottom $t\bar{t}$, $W^+ + \text{jets}$, and $W^- + \text{jets}$ are shown. For the parameters of the error functions a linear dependence on H_T is imposed. The points show the values of α obtained for individual bins in H_T . The solid lines correspond to fits to constant values of α in the control regions.

("smeared") to account for the finite detector resolution. The resolution depends on the hadronic activity and on the time-dependent running conditions. The response function for this E_T smearing can be obtained from QCD multijet events, which do not have a significant amount of true E_T [46]. A sample dominated by these events is selected using a set of triggers based only on H_T , and the response functions are extracted in bins of H_T , jet multiplicity, and b-jet multiplicity. In each H_T bin the shapes for different jet multiplicities are then combined according to the multiplicity distribution observed in the single-lepton dataset.

The convolution of the true E_T distribution with the response functions described above assumes that the contribution to E_T from missing particles is uncorrelated in direction with the E_T contribution arising from jet mismeasurements. Simulation indicates that the correlation coefficient between these two contributions is only 0.13, and ancillary studies confirm that the uncertainty on the prediction incurred by ignoring the correlation is negligible.

5.3 Estimation of the E_T spectrum from data

The full E_T model described in the previous subsections is used in a simultaneous fit to H_T bins in the subsamples defined by the three b-jet multiplicities, the two lepton flavors, and the two charges. The bin sizes in H_T are chosen to ensure adequate data in each bin. The parameters α resulting from the fits to data and to simulation are summarized in Table 1.

The predictions for each of the signal regions are obtained by integrating the E_T model in bins of H_T . In each H_T bin the E_T distribution is normalized to the observed number of events at $100 < E_T < 250$ GeV. The final estimate is obtained by summing over all H_T bins. The statistical uncertainty on the prediction for each signal region is evaluated by pseudo-experiments, repeating the prediction with values for α in the different categories sampled according to the central value and covariance matrix provided by the fit.

In Table 2 the predictions of the fit of the \cancel{E}_T model to simulated events are compared to the true values for regions defined by lower limits of 750 GeV and 1000 GeV on H_T , and of 250, 350, and 450 GeV on \cancel{E}_T . Good agreement is observed. The results from data are summarized in Section 7.

Table 1: Fit results for the parameter α from the control regions in data and simulation. The quoted uncertainties are statistical.

		W^+ +jets	W^- +jets	$t\bar{t}$
μ	data	0.676 ± 0.014	0.717 ± 0.024	0.818 ± 0.014
	simulation	0.641 ± 0.019	0.709 ± 0.024	0.819 ± 0.013
e	data	0.655 ± 0.015	0.697 ± 0.026	0.857 ± 0.016
	simulation	0.651 ± 0.013	0.736 ± 0.025	0.806 ± 0.013

Table 2: Predicted and true event counts in simulation for different signal regions. Uncertainties are statistical.

	750 < H_T < 2500 GeV		1000 < H_T < 2500 GeV			
	simulation		simulation			
	predicted	true	predicted	true		
$250 < \cancel{E}_T < 2000 \text{ GeV}$						
Total	196 ± 11	183.2 ± 5.1	52.0 ± 4.3	53.4 ± 2.7		
0 b tag	129.7 ± 8.6	113.4 ± 3.4	35.1 ± 3.6	31.5 ± 1.8		
1 b tag	47.4 ± 3.2	48.5 ± 3.1	11.3 ± 1.5	15.9 ± 1.7		
≥ 2 b tags	19.3 ± 1.9	21.2 ± 2.2	5.7 ± 1.0	6.0 ± 1.9		
$350 < \cancel{E}_T < 2000 \text{ GeV}$						
Total	74.5 ± 5.1	71.9 ± 2.9	21.9 ± 2.2	23.3 ± 1.7		
0 b tag	52.8 ± 4.4	48.1 ± 2.0	15.7 ± 1.8	13.6 ± 1.0		
1 b tag	16.2 ± 1.2	17.2 ± 1.7	4.3 ± 0.6	6.7 ± 1.1		
≥ 2 b tags	5.6 ± 0.6	6.7 ± 1.3	1.9 ± 0.3	3.0 ± 0.9		
$450 < \cancel{E}_T < 2000 \text{ GeV}$						
Total	28.1 ± 2.4	30.2 ± 1.8	9.5 ± 1.1	11.2 ± 1.1		
0 b tag	21.0 ± 2.1	21.1 ± 1.2	7.2 ± 1.0	7.2 ± 0.7		
1 b tag	5.5 ± 0.5	6.4 ± 0.9	1.7 ± 0.3	2.6 ± 0.6		
≥ 2 b tags	1.6 ± 0.2	2.7 ± 0.8	0.6 ± 0.1	1.4 ± 0.6		

5.4 Experimental systematic uncertainties

The results can be affected by systematic uncertainties, which arise from detector effects, assumptions made about the shape of the distribution, theoretical uncertainties, and the contamination due to other backgrounds. The impact of these uncertainties on the prediction can be quantified by a relative variation defined as $\delta\rho = (N'_{\text{pred}}/N'_{\text{true}})/(N_{\text{pred}}/N_{\text{true}}) - 1$ where N_{pred} (N_{true}) is the predicted (true) number of events and the prime denotes the values with the systematic effect included. For those uncertainties that only affect the estimation procedure but not the true number of events in the signal region, this amounts to the relative change in the prediction. For all other sources, $\delta\rho$ determines the variation in closure estimated with simulation, i.e., how well the prediction follows the change of events in the signal region.

Miscalibration of the jet energy scale (JES) leads to a modification of the true number of events in the signal region but is compensated to a large extent by a corresponding change in the predicted number of events. The effect due to the uncertainty on the JES is determined by shifting

the energy of jets with $p_T > 10 \text{ GeV}$ and $|\eta| < 4.7$ in simulated events up and down according to p_T - and η -dependent uncertainties that have been measured using dijet and $\gamma/Z+\text{jets}$ events [43]. The applied shifts, which are 1–3% for jets with $p_T > 40 \text{ GeV}$ and $|\eta| < 2.0$ and increase towards lower p_T and higher $|\eta|$, are propagated to the E_T result. The uncertainty on the energy of jets with $p_T < 10 \text{ GeV}$, referred to as unclustered energy, is assumed to be 10%. This uncertainty is also propagated to the E_T result assuming full correlation with the JES uncertainty. For the muon channel and a signal region inclusive in b-jet multiplicity and defined by $H_T > 1000 \text{ GeV}$ and $E_T > 250 \text{ GeV}$, the variations are +14% and –30%, respectively, while the systematic uncertainty $\delta\rho$ is 6%.

Lepton efficiencies are expected to have a small impact on the background prediction, because an overall change of scale is compensated by a corresponding change in the normalization regions, and the preselection cuts have been chosen to use only kinematic regions with stable trigger and reconstruction efficiencies. Therefore only small changes are expected in the ratios of yields between the signal and the normalization regions. In order to test the impact of a possible non-uniformity, the lepton efficiencies are lowered by 5% in the endcap regions and by a linear variation of –20% to 0% in the low p_T range of 20 to 40 GeV, where any residual effect of the efficiency in the threshold region would have the highest impact.

Over the course of the data collection period, the maximum instantaneous luminosity per bunch crossing and, hence, the average number of simultaneous collisions, changed dramatically. Simulated events are matched to the pileup conditions observed in data using the distribution of the number of reconstructed primary vertices, and the simulation provides a satisfactory description of the dependence of several key observables as a function of the number of simultaneous collisions. Possible residual effects are tested by varying the event weight according to the reconstructed number of primary vertices n_{vtx} by $\pm 5\% \times (n_{\text{vtx}} - \langle n_{\text{vtx}} \rangle)$ around the mean number $\langle n_{\text{vtx}} \rangle = 7$.

Differences between the efficiencies to tag b-quark, c-quark, and light-flavor jets in data and simulation are taken into account by applying p_T - and η -dependent scale factors to the simulated events. These scale factors are measured in data using QCD multijet event samples with uncertainties on the order of a few percent [44]. Variations in the efficiency and purity of the b-jet identification would move events among the three b-tag multiplicity bins and change the fractions of W+jets and t̄t events in each bin. The size of this effect is estimated by varying efficiencies and mistagging rates within the uncertainties. As expected, the determination of the fractions based on fits to the b-jet multiplicity compensates for these changes and the residual effects are small.

5.5 Model-related systematic uncertainties for the E_T templates method

The background estimation procedure is designed to provide individual estimates of the E_T distribution of each of the leading backgrounds: t̄t, W⁺+jets, and W[−]+jets. The accuracy of the separation between t̄t and W+jets events is tested by varying the t̄t and W+jets cross sections individually by one third. Moreover, the sensitivity of the fit results to the b-jet multiplicity distribution is estimated by varying the resulting ratio of W+jets to t̄t events by its uncertainty. The corresponding effect is small. The impact of other background sources, in particular of the contribution from dilepton events, is tested by varying the amount of all non-leading backgrounds by ±50%.

The uncertainty on the E_T model is tested by varying the β parameter by ±10% with respect to its nominal value of 0.5. This variation is motivated by the uncertainty from fitting β in single-lepton events with two jets. As shown in Fig. 4, the parameter α shows no significant

dependence on H_T . The uncertainty on this assumption is quantified by imposing a slope according to the uncertainties of the linear fits as a function of H_T in the control region. These two model-related effects constitute the dominant systematic uncertainties in the background estimation. For the parameters of the error functions b and c , 16 independent variations are considered in the eigenbasis of the parameters of the linear functions describing the evolution in H_T , and the model describing this evolution is changed from linear to quadratic. The effect of these variations is rather small, since the prediction for any signal region is a sum of many H_T bins, and the variations of the error function parameters tend to cancel each other.

An additional source of uncertainty is due to the W polarization, which would alter the \cancel{E}_T distribution for a given momentum of the W boson. In order to quantify this uncertainty we modify the generator-level polarization distributions in bins of lepton p_T and rapidity according to varied scenarios. The fit is performed for each of the modified datasets, and the highest $\delta\rho$ is then assigned as a systematic uncertainty.

The systematic uncertainties for the signal region defined by $H_T > 1000 \text{ GeV}$ and $\cancel{E}_T > 250 \text{ GeV}$ are presented in Tables 3 and 4. Table 3 contains all contributions that are not directly related to b-jet identification. They have been evaluated in a W+jets and a t̄t dominated subsample, defined as events without or with at least one identified b jet, respectively. Table 4 lists the b-tagging related systematic effects in the three b-jet multiplicity bins.

Table 3: Relative systematic uncertainties ($\delta\rho$) not directly related to b tagging for the background estimation in the signal region $1000 < H_T < 2500 \text{ GeV}$ and $250 < \cancel{E}_T < 2000 \text{ GeV}$.

Source	μ channel			e channel		
	Total	0 b tag	≥ 1 b tag	Total	0 b tag	≥ 1 b tag
Jet and \cancel{E}_T scale	6.0%	7.5%	7.2%	3.1%	5.6%	2.1%
Lepton efficiency	0.4%	0.3%	0.6%	0.6%	1.3%	0.7%
Pileup	0.1%	0.1%	0.2%	0.3%	1.5%	0.4%
W polarization	0.5%	0.6%	0.1%	1.3%	1.8%	0.3%
Non-leading backgrounds	0.7%	0.4%	0.4%	4.0%	3.0%	6.2%
Dilepton contribution	0.1%	0.5%	0.7%	0.6%	1.2%	0.6%
$\sigma(t\bar{t})$	1.2%	2.3%	1.6%	0.7%	1.8%	2.0%
$\sigma(W+\text{jets})$	1.3%	2.9%	2.3%	2.6%	1.6%	2.8%
Exponent $\beta t\bar{t}$	1.6%	0.2%	5.3%	1.8%	0.3%	4.8%
Exponent $\beta W^++\text{jets}$	3.5%	4.4%	1.3%	3.6%	4.6%	1.5%
Exponent $\beta W^-+\text{jets}$	0.7%	0.8%	0.3%	0.9%	1.4%	0.9%
α slope $t\bar{t}$	11.0%	2.4%	29.3%	14.8%	5.0%	34.3%
α slope $W^++\text{jets}$	15.9%	20.6%	6.0%	16.5%	22.2%	5.1%
α slope $W^-+\text{jets}$	4.9%	8.2%	2.0%	5.6%	8.7%	0.5%
Error function parameters	4.1%	4.6%	2.9%	3.1%	3.2%	2.7%

In simulated event samples, the background estimation procedure produces results that are compatible with the simulated rates. Conservatively, a systematic uncertainty using the maximum of the statistical uncertainty of this comparison and of the absolute value of the deviation is assigned. For the signal region mentioned above, this amounts to 5.9%. We also evaluate the effect of possible differences in the \cancel{E}_T distributions between the different b-tag bins. In order to test the sensitivity to possible deviations in the low- H_T control region used for the fit, we have evaluated the relative variations in the predictions for the 1 b-tag (≥ 2 b-tag) bin in data by repeating the fit without the ≥ 2 b-tag (1 b-tag) bin. The uncertainty in the ≥ 1 b-tag bin was set to the average of the variations in the 1 b-tag and ≥ 2 b-tag bins. For the signal region mentioned above, the uncertainties are 2.0%, 4.2%, and 8.5% for the 1 b-tag, ≥ 1 b-tag, and ≥ 2

Table 4: Relative systematic uncertainties related to b tagging in the signal region $1000 < H_T < 2500 \text{ GeV}$ and $250 < \cancel{E}_T < 2000 \text{ GeV}$.

Source	Total	0 b tag	1 b tag	≥ 1 b tag	≥ 2 b tags
μ channel					
W+jets/ $t\bar{t}$ ratio	2.9%	2.1%	6.1%	4.8%	2.4%
b-tagging efficiency	2.0%	1.5%	2.2%	1.3%	5.1%
Mistagging rate	0.4%	0.4%	0.7%	0.9%	0.6%
e channel					
W+jets/ $t\bar{t}$ ratio	1.1%	2.4%	2.6%	2.3%	2.3%
b-tagging efficiency	2.2%	1.6%	0.8%	1.7%	3.6%
Mistagging rate	0.3%	0.4%	0.4%	0.2%	0.1%

b-tag bins, respectively.

6 The Factorization Method

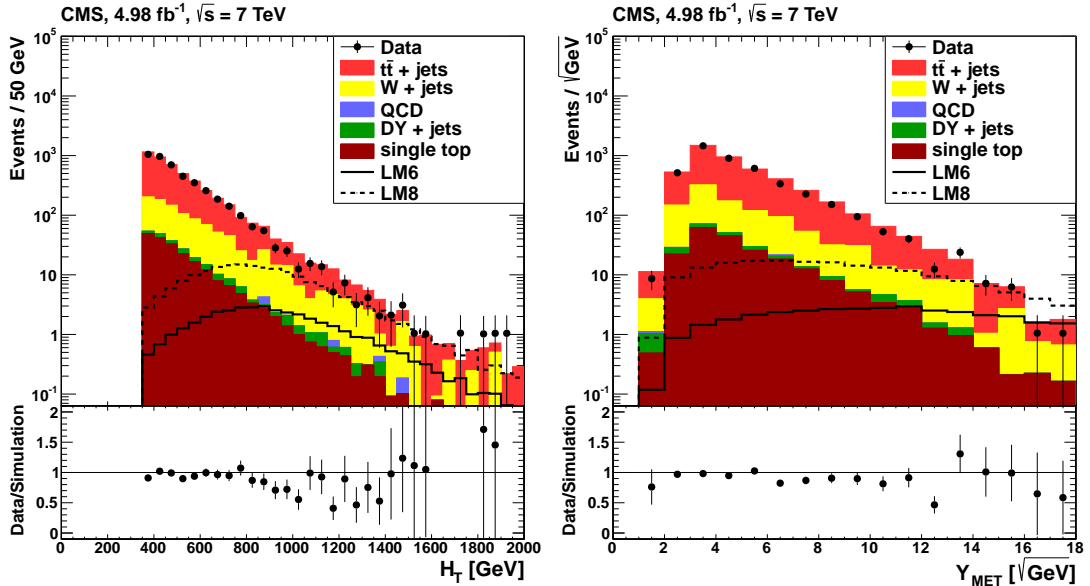


Figure 5: Distributions of (left) H_T and (right) Y_{MET} for data compared to the different SM processes. The muon and electron channels are combined and at least one b tag is required. The CMS data are represented by solid points and the simulated SM events by stacked histograms. The two lines represent possible signal scenarios. The simulation is normalized to the integrated luminosity of the data sample.

The factorization method is based on the variables H_T and Y_{MET} , which are shown for the inclusive 1 b-tag selection for data and simulated SM events in Fig. 5. The SM simulation lies systematically above the data, showing the need for background estimation from data. Since H_T and Y_{MET} are nearly uncorrelated for $t\bar{t}$ production, which constitutes the main background in events with at least one b jet, a factorization ansatz in the $Y_{\text{MET}}-H_T$ plane can be used to estimate the background contribution, namely from control regions with low H_T and/or Y_{MET} .

For the factorization method, a minimum of $H_T > 375 \text{ GeV}$ and $\cancel{E}_T > 60 \text{ GeV}$ is required together with at least four jets with $p_T > 40 \text{ GeV}$. For a precise estimation of the number of

background events in the signal region, it is essential to have enough events in the control regions. Therefore, the definition of the signal region depends on the number of required b tags. The analysis is performed, and results are presented, in three channels according to the number of b tags: 1, 2, and ≥ 3 b tags, selected with the track-counting algorithm. In addition we study the 0 b-tag bin for cross checks and use a combined ≥ 1 b-tags bin for limit setting in the CMSSM case. The signal region is defined as $H_T > 800 \text{ GeV}$ and $Y_{\text{MET}} > 5.5 \sqrt{\text{GeV}}$ for the 1, the 2, and the combined ≥ 1 b-tag bins, and $H_T > 600 \text{ GeV}$ and $Y_{\text{MET}} > 6.5 \sqrt{\text{GeV}}$ for the 0 and ≥ 3 b-tag bins. These regions are optimized to balance two opposing requirements: a small background contribution to the signal region but nonetheless enough background events in the three control regions that the statistical uncertainties on the background predictions are small.

The signal region is populated with events described by the tails of SM distributions and mis-measurement related to the finite detector resolution. The control regions (A , B , and C) and the

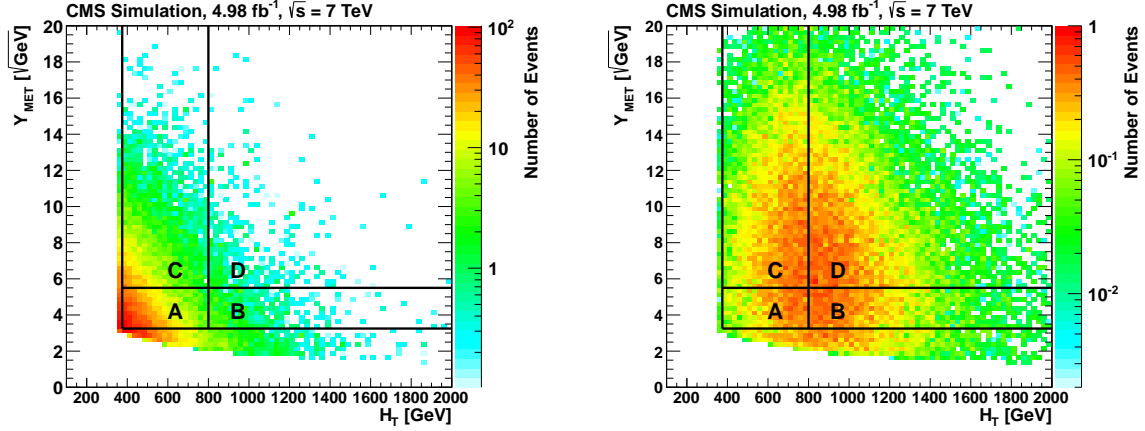


Figure 6: Distributions of Y_{MET} vs. H_T for (left) the SM background and (right) the SUSY LM8 scenario. The muon and electron channels are combined and at least one b tag is required.

signal region (D) used for the factorization method with H_T and Y_{MET} are defined in Table 5.

Table 5: Definition of the different regions used for the factorization method with H_T and Y_{MET} . Two sets of selections are defined depending on the number of b tags. Region D is expected to be signal dominated.

Region	b tags: 1, 2, ≥ 1		b tags: 0, ≥ 3	
	H_T/GeV	$Y_{\text{MET}}/\sqrt{\text{GeV}}$	H_T/GeV	$Y_{\text{MET}}/\sqrt{\text{GeV}}$
A	$375 - 800$	$3.25 - 5.5$	$375 - 600$	$3.25 - 6.5$
	> 800		> 600	
C	$375 - 800$		$375 - 600$	
	> 800	> 5.5	> 600	> 6.5

The number of background events \hat{N}_D in region D is estimated from the three control regions as:

$$\hat{N}_D = \kappa N_B \frac{N_C}{N_A}. \quad (2)$$

Were the two variables completely uncorrelated, the correlation factor κ would equal one. As

Y_{MET} and H_T have a small correlation, the factor κ is determined to be 1.20 with an overall uncertainty of about 11%, as discussed in Section 6.1.

The distribution of SM events in the $Y_{\text{MET}} - H_T$ plane after the event selection in the combined muon and electron channel with the requirement of at least one b tag is presented in Fig. 6(a). The corresponding results for the LM8 SUSY scenario are presented in Fig. 6(b). It is observed that the SM events are mainly located in the control regions, while the signal events are present in the signal and the control regions. The signal contamination is taken into account in the likelihood model for the scans during limit setting.

6.1 Systematic uncertainties for the factorization method

As for the \cancel{E}_T template method, many systematic effects result in small uncertainties only, since the background prediction is affected in the same way as the measurements.

Values of κ as defined in Eq. (2) for the main SM background processes are shown in Table 6 for both signal region definitions and different numbers of b tags. For the dominant background, due to $t\bar{t}$ events, as well as for the backgrounds from single-top and $W+\text{jets}$ events, the correlations are larger than one, indicating a residual correlation. Besides these processes we expect only small contributions from $Z+\text{jets}$ events. The stability of the correlation factor κ has been tested extensively, and the observed correlation is accounted for by the value of κ from simulation. To account for uncertainties in the cross sections of the main SM processes, each cross section is scaled up and down by 50%, and the corresponding uncertainty on κ is determined.

Table 6: Correlation factor κ between H_T and Y_{MET} for the main SM background processes and a for different number of b tags, for the two signal regions. For purposes of illustration, the corresponding results for a sample with 0 b tags is also shown. While the 0 b-tag sample is dominated by $W+\text{jets}$ events, the channels that include b tags contain mainly $t\bar{t}$ events. Only statistical uncertainties are shown.

Signal region	No. of b tags	$\kappa (t\bar{t})$	$\kappa (\text{single top})$	$\kappa (W+\text{jets})$	$\kappa (\text{all SM})$
$H_T > 800 \text{ GeV}$ $Y_{\text{MET}} > 5.5 \sqrt{\text{GeV}}$	1 b-tag	1.16 ± 0.02	1.14 ± 0.14	1.17 ± 0.05	1.19 ± 0.03
	2 b-tags	1.22 ± 0.02	1.25 ± 0.16	1.24 ± 0.10	1.23 ± 0.02
	≥ 1 b-tags	1.18 ± 0.01	1.18 ± 0.10	1.18 ± 0.04	1.20 ± 0.02
$H_T > 600 \text{ GeV}$ $Y_{\text{MET}} > 6.5 \sqrt{\text{GeV}}$	0 b-tags	1.14 ± 0.06	1.44 ± 0.49	1.25 ± 0.04	1.25 ± 0.04
	≥ 3 b-tags	1.17 ± 0.02	1.40 ± 0.18	1.24 ± 0.19	1.19 ± 0.02

Except for the \cancel{E}_T requirement, the offline selection criteria are designed to be well above the trigger thresholds, where the efficiency reaches a plateau. For events with $\cancel{E}_T < 80 \text{ GeV}$, the efficiency of the triggers with a H_T^{trigger} threshold of 40 GeV can be as low as around 80%. In these cases the prediction is corrected to account for the inefficiencies.

As the studies above are based on simulation, a cross-check is performed with data in the 0 b-tag channel, which can be considered as signal-free, since previous analyses have already excluded this part of phase space [36]. From this channel a value of $\kappa = 1.19 \pm 0.13$ is observed in data, while for the SM simulation a value of 1.25 ± 0.04 is extracted. Although the values are consistent within their statistical uncertainties, a smaller value of κ cannot be excluded. We account for this possibility by including an additional systematic uncertainty of 10% on the value of κ . The uncertainties for the different selections are described in Section 5.4 and summarized in Table 7. The statistical uncertainty in simulation is relatively small, as the b tagging is applied in the simulation by event weights. In addition, the simulated jet energy resolution (JER) [43] of jets with $p_T > 10 \text{ GeV}$ and $|\eta| < 4.7$ is globally increased by 10% to

provide a more realistic description of the data. The uncertainty on the jet energy resolution is then determined by variation of the corrected simulated JER up and down by $\pm 10\%$, and propagated to \cancel{E}_T .

Table 7: Overview of the uncertainties on the correlation factor κ for the different b-tag selections. The signal regions corresponding to the number of required b tags are as defined in Table 5. All systematic uncertainties are added in quadrature. The variations in JES, JER, p_T^{lepton} , and unclustered energy are propagated to the \cancel{E}_T . The row labeled ‘0 b tag’ addresses the difference between the values of κ in data and simulation.

Variation	$\Delta\kappa$ (0 b tags)	$\Delta\kappa$ (1 b tag)	$\Delta\kappa$ (2 b tags)	$\Delta\kappa$ (≥ 3 b tags)	$\Delta\kappa$ (≥ 1 b tag)
JES	2.0%	2.7%	1.3%	0.4%	2.0%
JER	1.1%	2.1%	3.0%	1.5%	2.4%
p_T^{lepton}	1.2%	1.5%	1.7%	1.2%	1.6%
Unclustered energy	0.5%	0.5%	1.1%	0.4%	0.8%
Pileup	0.7%	0.6%	0.8%	1.9%	0.7%
b-tagging scale factor	0.1%	0.2%	0.3%	0.3%	< 0.1%
Mistagging scale factor	0.1%	0.1%	0.2%	0.2%	< 0.1%
Cross section variation	3.4%	1.0%	2.0%	1.4%	0.4%
0 b tag	10.0%	10.0%	10.0%	10.0%	10.0%
Total uncertainty	10.9%	10.7%	10.9%	10.2%	10.7%
Statistical uncertainty	3.8%	3.7%	2.5%	2.1%	2.3%

Since the value of κ is found to be consistent for all channels within the statistical uncertainties, we use the value $\kappa = 1.20 \pm 0.02$ (stat) found for simulated events with ≥ 1 b-tag to describe all channels. The corresponding systematic uncertainty for each channel is taken from Table 7. The sum of the statistical and systematic uncertainty on κ corresponds to the systematic uncertainty for the prediction \hat{N}_D .

For the comparison of data with simulation, the absolute uncertainties for the signal and SM background, and the scale factors between data and simulation, need to be taken into account. These scale factors correct for the differences in the lepton identification efficiency, b-tagging efficiency, and pileup as described in Sections 3 and 5.4. The effect of the b-tagging efficiency is investigated by scaling the scale factors up and down in simulated events. This is performed separately for the b-tagging efficiency scale factor and the mistagging rate scale factor. Since triggers are not used in the simulation, scale factors are applied to account for the trigger efficiencies when the simulation is compared to data. An additional uncertainty of 0.2% accounts for the trigger efficiency correction for the prediction in data. The product of all scale factors differs from one by at most ten percent.

Model uncertainties are also taken into account. For the dominant $t\bar{t}$ background, the uncertainties for the inclusive cross section are calculated using the Monte Carlo for femtobarn processes (MCFM 5.8) [47]. The uncertainties associated with scales are determined by separately varying the factorization and matching scales by a factor of 2 up and down. Including parton distribution function (PDF) uncertainties [48], we apply a total uncertainty of 16%.

The uncertainties for SM simulation in signal region D , shown in Table 8, are needed for the comparison of data with the SM simulation (as shown in Section 7), but are not used in the limit determination with the scans.

Table 8: Systematic uncertainties in the signal region for the different selections for the SM simulation, needed for the comparison with data (as in Table 10). The signal regions corresponding to the number of required b tags are as defined in Table 5. All uncertainties are summed in quadrature. The variations in JES, JER, p_T^{lepton} , and unclustered energy are propagated to the \cancel{E}_T .

Variation	ΔN_D (0 b tags)	ΔN_D (1 b tag)	ΔN_D (2 b tags)	ΔN_D (≥ 3 b tags)	ΔN_D (≥ 1 b tag)
JES	17.8%	16.7%	19.2%	17.3%	17.5%
JER	17.1%	4.8%	6.2%	5.4%	5.3%
p_T^{lepton}	0.6%	2.4%	2.1%	2.5%	1.9%
Unclustered energy	0.1%	0.9%	1.1%	0.5%	1.0%
Pileup	2.7%	2.2%	0.8%	1.1%	1.6%
b-tagging scale factor	2.6%	1.2%	4.1%	7.8%	1.5%
Mistagging scale factor	2.0%	0.8%	1.3%	5.9%	1.3%
Model uncertainty	16.0%	16.0%	16.0%	16.0%	16.0%
Lepton trigger & ID	3.0%	3.0%	3.0%	3.0%	3.0%
Luminosity uncertainty	2.2%	2.2%	2.2%	2.2%	2.2%
Total uncertainty	30.0%	26.7%	26.5%	24.4%	24.8%
Statistical uncertainty	11.0%	8.3%	8.6%	3.4%	5.6%

7 Results

The background estimation methods described in Sections 5 and 6 are used to predict the SM contribution to the signal regions.

A graphical representation of the \cancel{E}_T spectra estimated with the template method in a background-dominated region at low H_T and the two signal regions at high H_T are shown in Fig. 7. The fit provides a good description of the observed spectrum in the control region, and no excess is observed at high H_T . The numerical results for different signal regions are summarized in Table 9, along with the observed event counts and the expectations for the two SUSY benchmark scenarios LM6 and LM8. No events are observed above the common upper boundaries of the signal regions of $H_T < 2.5$ TeV and $\cancel{E}_T < 2$ TeV.

For the factorization method, the number of events in the signal region N_D and the predicted value \hat{N}_D are summarized in Table 10, which additionally includes expectations for the SM and for the SM with contributions of the LM6 and LM8 SUSY scenarios added. The measured number of events N_D and the predicted value \hat{N}_D are in agreement and no excess is observed. The reconstructed number of events in region D and the predicted value \hat{N}_D are in agreement also for the SM simulation, showing the validity of the factorization ansatz for the background estimation. For the comparison of data and simulation, several scale factors are taken into account, as described in Section 6.1. The uncertainty on the number of events N_D for the SM prediction from simulation is larger than that on the prediction \hat{N}_D from data, showing the advantage of this background estimation method.

8 Interpretation

Using the results presented in Section 7, limits are set on the parameters of several supersymmetric models, including the CMSSM and the simplified model described in Section 3.

Limits are set using the CL_s method [49, 50] with a test statistic given by a profile likelihood ra-

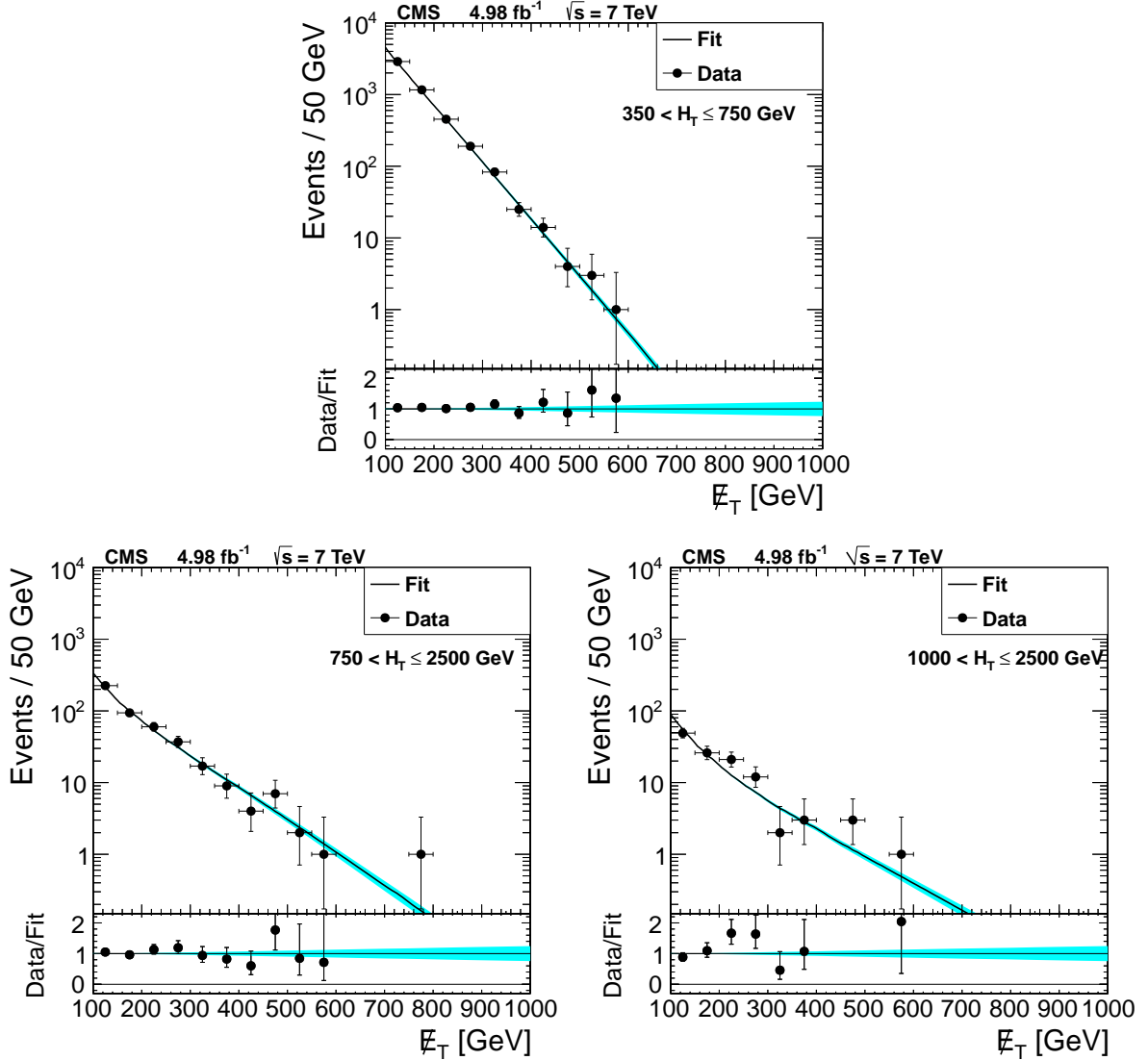


Figure 7: Distribution of E_T in the muon channel: data (points) and fit result of the template method (line) for (top) $350 < H_T < 750 \text{ GeV}$; data and prediction obtained from the fit for (bottom left) $750 < H_T < 2500 \text{ GeV}$ and for (bottom right) $1000 < H_T < 2500 \text{ GeV}$. The bands around the fit correspond to the statistical uncertainty on the parameter α . The systematic uncertainties have been calculated for $E_T > 250, 350$ and 450 GeV and range from $16 - 32\%$ ($24 - 42\%$) for $H_T > 750$ (1000) GeV as reported in Tab. 9. The lower panels show the ratio between the fitted model and data.

Table 9: Predicted and observed yields from the \cancel{E}_T -template method for the different signal regions. The first uncertainties are statistical and the second systematic. The expected yields and statistical uncertainties for the two benchmark points LM6 and LM8 are shown for comparison.

	observed	predicted	stat.	sys.	LM6	LM8
$750 < H_T < 2500 \text{ GeV}, 250 < \cancel{E}_T < 2000 \text{ GeV}$						
Total	137	146	± 9	± 24	42.2	± 6.5
0 b tag	97	99	± 8	± 18	26.3	± 5.1
1 b tag	35	34.6	± 2.8	± 7.5	10.7	± 3.3
≥ 1 b tag	40	47	± 3	± 10	16.0	± 4.0
≥ 2 b tags	5	12.3	± 1.4	± 2.7	5.2	± 2.3
$750 < H_T < 2500 \text{ GeV}, 350 < \cancel{E}_T < 2000 \text{ GeV}$						
Total	44	54	± 5	± 12	30.7	± 5.5
0 b tag	32	38.7	± 3.6	± 9.5	19.9	± 4.5
1 b tag	11	11.5	± 1.0	± 3.5	7.5	± 2.7
≥ 1 b tag	12	14.8	± 1.1	± 4.5	10.9	± 3.3
≥ 2 b tags	1	3.3	± 0.4	± 1.0	3.3	± 1.8
$750 < H_T < 2500 \text{ GeV}, 450 < \cancel{E}_T < 2000 \text{ GeV}$						
Total	20	19.6	± 2.1	± 6.2	19.6	± 4.4
0 b tag	14	14.9	± 1.7	± 5.2	13.3	± 3.7
1 b tag	5	3.8	± 0.4	± 1.5	4.5	± 2.1
≥ 1 b tag	6	4.7	± 0.4	± 1.8	6.3	± 2.5
≥ 2 b tags	1	0.9	± 0.1	± 0.3	1.8	± 1.3
$1000 < H_T < 2500 \text{ GeV}, 250 < \cancel{E}_T < 2000 \text{ GeV}$						
Total	36	37.5	± 3.7	± 8.9	18.1	± 4.3
0 b tag	30	27.0	± 3.2	± 7.0	10.9	± 3.3
1 b tag	5	7.5	± 1.2	± 2.6	4.8	± 2.2
≥ 1 b tag	6	10.5	± 1.3	± 3.6	7.2	± 2.7
≥ 2 b tags	1	3.0	± 0.6	± 1.0	2.3	± 1.5
$1000 < H_T < 2500 \text{ GeV}, 350 < \cancel{E}_T < 2000 \text{ GeV}$						
Total	13	15.5	± 1.7	± 4.9	13.0	± 3.6
0 b tag	11	11.7	± 1.6	± 4.2	8.1	± 2.8
1 b tag	2	2.9	± 0.5	± 1.4	3.4	± 1.9
≥ 1 b tag	2	3.8	± 0.5	± 1.8	4.9	± 2.2
≥ 2 b tags	0	1.0	± 0.2	± 0.5	1.5	± 1.2
$1000 < H_T < 2500 \text{ GeV}, 450 < \cancel{E}_T < 2000 \text{ GeV}$						
Total	7	6.6	± 0.9	± 2.8	8.5	± 2.9
0 b tag	6	5.2	± 0.8	± 2.3	5.5	± 2.3
1 b tag	1	1.1	± 0.2	± 0.7	2.1	± 1.5
≥ 1 b tag	1	1.4	± 0.2	± 0.9	3.0	± 1.7
≥ 2 b tags	0	0.3	± 0.1	± 0.2	0.8	± 0.9

tio. The likelihood function includes a Poisson distribution describing the number of observed events in the signal region. Its mean value is $B + \mu S$, where B is the predicted background, S the expected signal yield at the nominal cross section of the model under study, and μ the signal strength parameter.

For the \cancel{E}_T template method, $B = B_N r / (1 + \mu c)$, where B_N is the background in the normalization region, r the ratio of the background in signal and normalization regions, determined by the \cancel{E}_T model, and c is the relative bias in the background estimation due to signal contamination. The effect of signal contamination is determined by repeating the background estimation on simulated samples combining SM processes and a signal at the nominal cross section. The nuisance parameter B_N is constrained by a second Poisson distribution with mean B_N , describing the number of observed events in the normalization region. For the factorization method, $B = \kappa B_B B_C / B_A$. The nuisance parameters B_i describing the estimated background in the three

Table 10: Number of reconstructed (N_D) and predicted (\hat{N}_D) events in the signal region for the factorization method for the SM, two possible signal scenarios (LM6, LM8), and data. The first uncertainties are statistical and the second systematic. The systematic uncertainty on \hat{N}_D in data is equal to the uncertainty on κ . The systematic uncertainty in simulation includes the uncertainty on the absolute rate of simulated events, as discussed in the text. The exclusive 0 b-tag selection is shown for comparison as well.

Signal region	Sample	N_D	\hat{N}_D
0 b-tags $H_T > 600 \text{ GeV}$ $Y_{\text{MET}} > 6.5 \sqrt{\text{GeV}}$	$\Sigma \text{ SM}$	$182 \pm 22 \pm 55$	$186 \pm 19 \pm 40$
	$\Sigma \text{ SM+LM6}$	$221 \pm 22 \pm 59$	$191 \pm 19 \pm 40$
	$\Sigma \text{ SM+LM8}$	$218 \pm 24 \pm 61$	$194 \pm 20 \pm 41$
	Data	155	$162 \pm 11 \pm 18$
1 b-tag $H_T > 800 \text{ GeV}$ $Y_{\text{MET}} > 5.5 \sqrt{\text{GeV}}$	$\Sigma \text{ SM}$	$74 \pm 5 \pm 18$	$74 \pm 4 \pm 14$
	$\Sigma \text{ SM+LM6}$	$95 \pm 5 \pm 21$	$77 \pm 4 \pm 14$
	$\Sigma \text{ SM+LM8}$	$132 \pm 6 \pm 29$	$90 \pm 5 \pm 16$
	Data	51	$53.9 \pm 6.3 \pm 5.9$
2 b-tags $H_T > 800 \text{ GeV}$ $Y_{\text{MET}} > 5.5 \sqrt{\text{GeV}}$	$\Sigma \text{ SM}$	$50 \pm 3 \pm 13$	$47.5 \pm 2.1 \pm 8.1$
	$\Sigma \text{ SM+LM6}$	$62 \pm 3 \pm 15$	$49.0 \pm 2.2 \pm 8.2$
	$\Sigma \text{ SM+LM8}$	$103 \pm 5 \pm 24$	$62.7 \pm 2.7 \pm 9.7$
	Data	27	$36.0 \pm 5.1 \pm 4.0$
≥ 3 b-tags $H_T > 600 \text{ GeV}$ $Y_{\text{MET}} > 6.5 \sqrt{\text{GeV}}$	$\Sigma \text{ SM}$	$22.6 \pm 1.1 \pm 6.0$	$21.3 \pm 0.9 \pm 4.0$
	$\Sigma \text{ SM+LM6}$	$27.1 \pm 1.1 \pm 6.6$	$21.9 \pm 0.9 \pm 4.1$
	$\Sigma \text{ SM+LM8}$	$66 \pm 4 \pm 15$	$34.3 \pm 1.8 \pm 4.8$
	Data	10	$13.8 \pm 3.2 \pm 1.5$
≥ 1 b-tag $H_T > 800 \text{ GeV}$ $Y_{\text{MET}} > 5.5 \sqrt{\text{GeV}}$	$\Sigma \text{ SM}$	$136 \pm 6 \pm 34$	$134 \pm 5 \pm 24$
	$\Sigma \text{ SM+LM6}$	$172 \pm 6 \pm 39$	$139 \pm 5 \pm 24$
	$\Sigma \text{ SM+LM8}$	$280 \pm 8 \pm 63$	$177 \pm 6 \pm 28$
	Data	84	$98 \pm 8 \pm 11$

control regions A, B, and C are constrained by three additional Poisson distributions with mean values $B_i + \mu \alpha_i S$, where i is the index of a control region. The second term describes the expected contribution of the signal to the control region and ensures a correct estimate in the presence of signal contamination. The full likelihood function contains additional log-normal terms describing the nuisance parameters affecting the expected signal yields and the parameters r and κ for the \cancel{E}_T template and the factorization method, respectively, corresponding to the different sources of systematic uncertainties.

The expected signal yields and systematic uncertainties are evaluated for every signal point in the parameter planes of the two models considered. Sources of experimental uncertainties on the signal selection include the jet energy and \cancel{E}_T scales, b-tagging efficiencies, and mistagging rates. These uncertainties are treated as fully correlated with the corresponding variations in the background estimate. Smaller contributions to the signal uncertainty are due to the lepton and trigger selection efficiencies and to the measurement of the luminosity (2.2%). In the likelihood function used for the factorization method, the correlation of uncertainties between the four regions is taken into account.

8.1 CMSSM

Within the CMSSM limits are set in the $m_{1/2}$ vs. m_0 plane with parameters $\tan \beta = 10$, $A_0 = 0 \text{ GeV}$, and $\mu > 0$. The acceptance and efficiency factors $\epsilon_i \mathcal{A}_i$ are calculated in a scan over the parameters m_0 and $m_{1/2}$. This is done with leading order (LO) simulation, combined with

next-to-leading order (NLO) and next-to-leading log (NLL) K -factors [51–55] for each SUSY subprocess separately. The experimental uncertainties on the signal selection efficiency are dominated by the jet and \cancel{E}_T energy scales. In the relevant region of the parameter plane, these variations are smaller than 20% for both methods. The contributions due to the lepton and trigger selection are about 5%.

For the \cancel{E}_T template method, the CMSSM limits are set in a multichannel approach using the 0 b-tag, 1 b-tag, and ≥ 2 b-tag bins, while for the factorization method at least one b tag is required. In the multichannel approach, the statistical uncertainties on the background estimation due to fluctuations in the normalization regions are treated as uncorrelated. Correlations between b-jet multiplicity bins in the \cancel{E}_T template method are evaluated for the uncertainties related to the \cancel{E}_T shape parameters. Variations in the b-jet identification efficiencies also lead to correlation between different bins and between signal yields and background predictions. All other systematic effects are treated as fully correlated.

The 95% confidence level (CL) limit using the CL_s technique is presented in Fig. 8, where the region below the black curves is excluded. The regions in H_T and \cancel{E}_T with the highest sensitivity are used: $H_T > 1000 \text{ GeV}$ and $\cancel{E}_T > 250 \text{ GeV}$ for the \cancel{E}_T template method, and $H_T > 800 \text{ GeV}$, $Y_{\text{MET}} > 5.5 \sqrt{\text{GeV}}$, and ≥ 1 b tag for the factorization method. Theoretical uncertainties on cross sections, arising from scale and PDF uncertainties, are illustrated by bands of the expected and observed limits with these uncertainties added or subtracted [56]. The \cancel{E}_T template method with the simultaneous use of three b-jet multiplicity bins provides the best expected limit.

8.2 Simplified model interpretation

In simplified models a limited set of hypothetical particles is introduced to produce a given topological signature [23–25]. The final state of the simplified model studied here contains a lepton and b jets as described in Section 3. The model has no intermediate mass state, so it contains only two free parameters: the mass of the LSP and the mass of the gluino. The signal cross sections are calculated up to NLO + NLL accuracy [51–56]. For each point in the parameter plane, the acceptance times efficiency and a cross section upper-limit is calculated. The systematic uncertainties are, as in the CMSSM case, determined for each point. The acceptance times the efficiency is presented in Fig. 9 for both background estimation methods.

For the \cancel{E}_T template method, the best expected limits for this model are obtained in the ≥ 2 b-tag bin. Cross section limits at 95% CL are calculated using the statistical framework described above. The signal region defined by the lower boundaries $H_T > 750 \text{ GeV}$ and $\cancel{E}_T > 250 \text{ GeV}$ is used. This choice results in high signal efficiencies also for low gluino masses and small mass differences between the gluino and the LSP. The limit with the factorization method is set requiring ≥ 3 b tags. In this case the signal region is defined as $H_T > 600 \text{ GeV}$ and $Y_{\text{MET}} > 6.5 \sqrt{\text{GeV}}$.

The effect of signal contamination on the background estimation is found to be higher than in the CMSSM case, with values up to 30%. This bias is taken into account in the calculation of the limits, which are shown in Fig. 10.

The analyses have also been tested on a simplified model describing direct stop pair production. Despite a higher acceptance times efficiency for this model, no limits can be obtained due to the low cross section of this process.

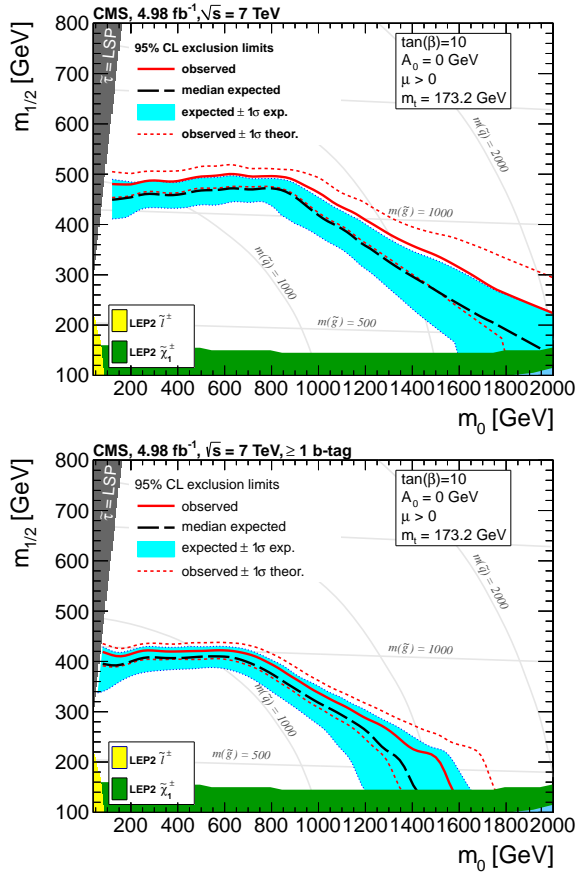


Figure 8: The 95% CL limit using the CL_s technique for the CMSSM model with $\tan\beta = 10$, $A_0 = 0$ GeV, and $\mu > 0$ (left) for the E_T template method using the multichannel approach and (right) for the factorization method requiring at least one b tag. The solid red line corresponds to the median expected limit, including all experimental uncertainties. The area below the solid red line (observed limit) is excluded, with the thin red dashed lines showing the effect of a variation of the signal yields due to theoretical uncertainties. The thick black dashed line shows the expected limit. It is surrounded by a shaded area representing the experimental uncertainties.

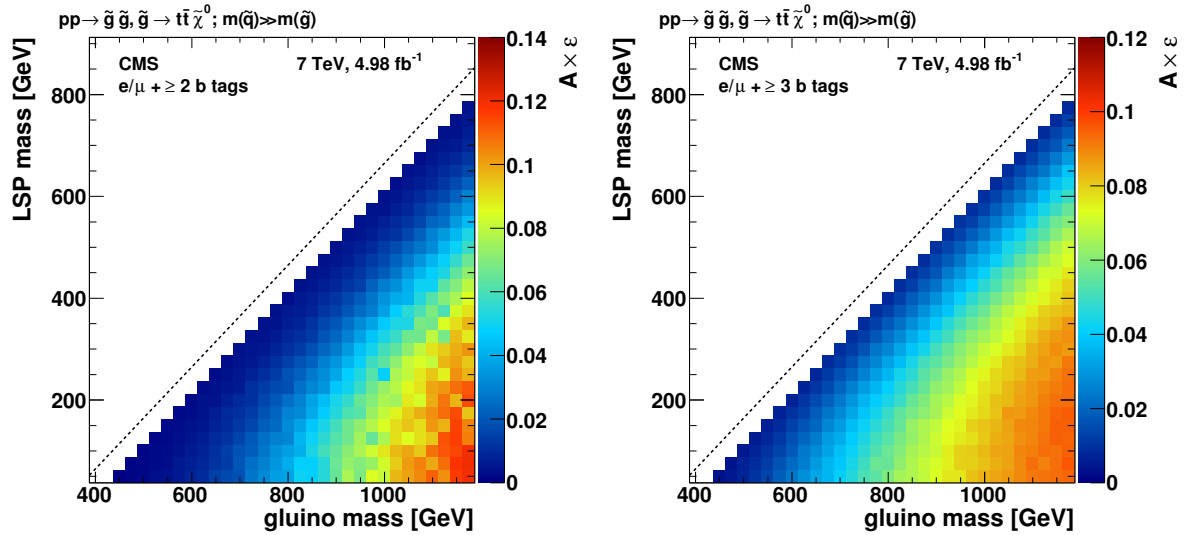


Figure 9: Acceptance times efficiency for the simplified model shown in Fig. 1 for (left) the \cancel{E}_T template method, where at least two b tags are required, and (right) the factorization method with three or more b tags. The diagonal dashed line marks the lower kinematical limit of the LSP mass.

9 Summary

A sample of events with a single electron or muon, multiple energetic jets, including identified b jets, and significant missing transverse energy, has been used to perform a search for new physics motivated by R -parity conserving supersymmetric models. The study is based on a data sample of proton-proton collision data recorded at $\sqrt{s} = 7$ TeV with the CMS detector, corresponding to an integrated luminosity of 4.98 fb^{-1} . The dominant standard model backgrounds are due to $t\bar{t}$ and $W+\text{jets}$ production.

Background contributions to different signal regions have been estimated from data with two complementary approaches. The first approach uses data in a control region at low H_T to determine templates of the \cancel{E}_T spectra for each of the main background components. Fits are performed simultaneously for three subsamples with 0, 1, and ≥ 2 identified b jets to determine the templates. Based on the templates and the observed number of events in a normalization region at low \cancel{E}_T , predictions are made for several signal regions at high H_T and \cancel{E}_T . The second approach uses the low correlation between H_T and $Y_{\text{MET}} = \cancel{E}_T / \sqrt{H_T}$. The standard model background in signal regions at high values of H_T and Y_{MET} is estimated based on the observed yields in three control regions. The two background estimation methods are complementary, as they have only small overlap in their control and signal regions, both in the standard model and in the signal scenarios.

No excess has been observed, and the results have been used to set 95% CL exclusion limits for several models. In the context of the constrained minimal supersymmetric extension of the standard model with parameters $\tan \beta = 10$, $A_0 = 0 \text{ GeV}$, and $\mu > 0$, the template method with the simultaneous use of the 0, 1, and ≥ 2 b-jet bins shows the highest sensitivity. Values of $m_{1/2}$ below about 450 GeV are excluded for m_0 in the range of about 200 GeV to about 800 GeV.

Limits have also been set in the parameter plane of the gluino and LSP masses of a simplified model that features four top quarks in the final state. Due to the high number of b quarks in the final state, the factorization method, which provides a background estimate for events with at

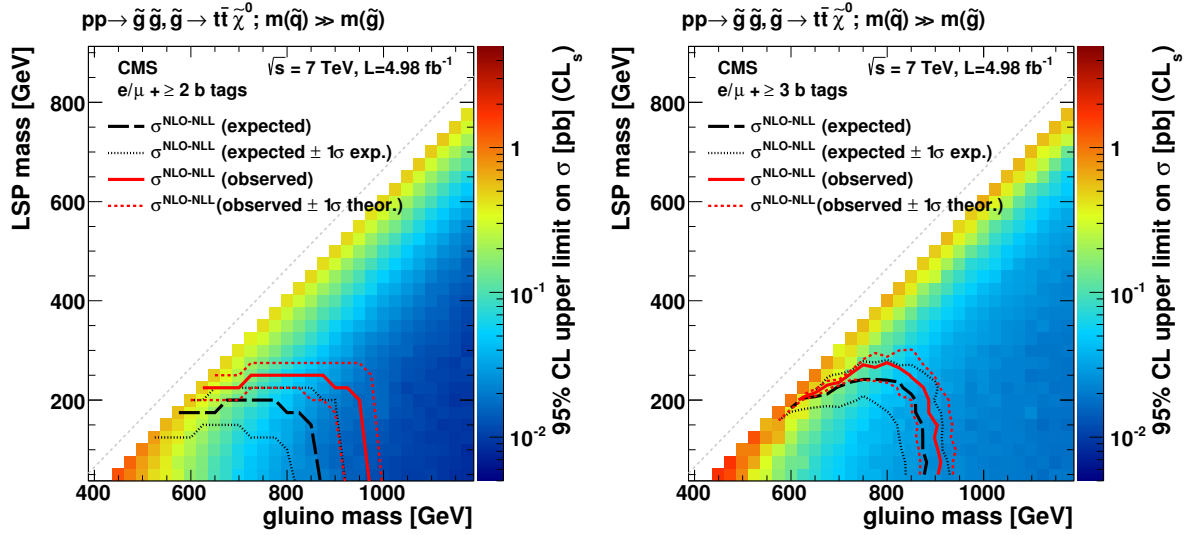


Figure 10: The 95% CL upper limit on the cross section using the CL_s technique for the simplified model shown in Fig. 1 for (left) the \cancel{E}_T template method, where at least two b tags are required, and (right) the factorization method with three or more b tags. The area below the thick solid red line is excluded. The thick dashed black line represents the expected limit. The diagonal dashed line marks the lower kinematical limit of the LSP mass.

least three identified b jets, has the highest sensitivity. Using the SUSY production cross section as a reference, the exclusion reaches to gluino masses of about 870 GeV. At a gluino mass of 750 GeV, LSP masses below 240 GeV are excluded. This is the first CMS analysis of this scenario in the final state with a single lepton and b-tagged jets. A similar mass range is excluded by other CMS analyses based on 2011 data [14–16]. Direct stop pair production can not yet be excluded with this analysis due to its low cross section.

Acknowledgements

We congratulate our colleagues in the CERN accelerator departments for the excellent performance of the LHC and thank the technical and administrative staffs at CERN and at other CMS institutes for their contributions to the success of the CMS effort. In addition, we gratefully acknowledge the computing centres and personnel of the Worldwide LHC Computing Grid for delivering so effectively the computing infrastructure essential to our analyses. Finally, we acknowledge the enduring support for the construction and operation of the LHC and the CMS detector provided by the following funding agencies: the Austrian Federal Ministry of Science and Research; the Belgian Fonds de la Recherche Scientifique, and Fonds voor Wetenschappelijk Onderzoek; the Brazilian Funding Agencies (CNPq, CAPES, FAPERJ, and FAPESP); the Bulgarian Ministry of Education, Youth and Science; CERN; the Chinese Academy of Sciences, Ministry of Science and Technology, and National Natural Science Foundation of China; the Colombian Funding Agency (COLCIENCIAS); the Croatian Ministry of Science, Education and Sport; the Research Promotion Foundation, Cyprus; the Ministry of Education and Research, Recurrent financing contract SF0690030s09 and European Regional Development Fund, Estonia; the Academy of Finland, Finnish Ministry of Education and Culture, and Helsinki Institute of Physics; the Institut National de Physique Nucléaire et de Physique des Particules / CNRS, and Commissariat à l’Énergie Atomique et aux Énergies Alternatives / CEA, France; the Bundesministerium für Bildung und Forschung, Deutsche Forschungsgemeinschaft,

and Helmholtz-Gemeinschaft Deutscher Forschungszentren, Germany; the General Secretariat for Research and Technology, Greece; the National Scientific Research Foundation, and National Office for Research and Technology, Hungary; the Department of Atomic Energy and the Department of Science and Technology, India; the Institute for Studies in Theoretical Physics and Mathematics, Iran; the Science Foundation, Ireland; the Istituto Nazionale di Fisica Nucleare, Italy; the Korean Ministry of Education, Science and Technology and the World Class University program of NRF, Korea; the Lithuanian Academy of Sciences; the Mexican Funding Agencies (CINVESTAV, CONACYT, SEP, and UASLP-FAI); the Ministry of Science and Innovation, New Zealand; the Pakistan Atomic Energy Commission; the Ministry of Science and Higher Education and the National Science Centre, Poland; the Fundação para a Ciência e a Tecnologia, Portugal; JINR (Armenia, Belarus, Georgia, Ukraine, Uzbekistan); the Ministry of Education and Science of the Russian Federation, the Federal Agency of Atomic Energy of the Russian Federation, Russian Academy of Sciences, and the Russian Foundation for Basic Research; the Ministry of Science and Technological Development of Serbia; the Secretaría de Estado de Investigación, Desarrollo e Innovación and Programa Consolider-Ingenio 2010, Spain; the Swiss Funding Agencies (ETH Board, ETH Zurich, PSI, SNF, UniZH, Canton Zurich, and SER); the National Science Council, Taipei; the Thailand Center of Excellence in Physics, the Institute for the Promotion of Teaching Science and Technology and National Electronics and Computer Technology Center; the Scientific and Technical Research Council of Turkey, and Turkish Atomic Energy Authority; the Science and Technology Facilities Council, UK; the US Department of Energy, and the US National Science Foundation.

Individuals have received support from the Marie-Curie programme and the European Research Council (European Union); the Leventis Foundation; the A. P. Sloan Foundation; the Alexander von Humboldt Foundation; the Belgian Federal Science Policy Office; the Fonds pour la Formation à la Recherche dans l’Industrie et dans l’Agriculture (FRIA-Belgium); the Agentschap voor Innovatie door Wetenschap en Technologie (IWT-Belgium); the Ministry of Education, Youth and Sports (MEYS) of Czech Republic; the Council of Science and Industrial Research, India; the Compagnia di San Paolo (Torino); and the HOMING PLUS programme of Foundation for Polish Science, cofinanced from European Union, Regional Development Fund.

References

- [1] S. P. Martin, “A Supersymmetry Primer”, (1997). [arXiv:hep-ph/9709356v6](https://arxiv.org/abs/hep-ph/9709356v6).
- [2] C. J. Flacco et al., “Direct Mass Limits for Chiral Fourth-Generation Quarks in All Mixing Scenarios”, *Phys. Rev. Lett.* **105** (2010) 111801, doi:[10.1103/PhysRevLett.105.111801](https://doi.org/10.1103/PhysRevLett.105.111801), arXiv:[1005.1077](https://arxiv.org/abs/1005.1077).
- [3] T. Han et al., “Phenomenology of the little Higgs model”, *Phys. Rev. D* **67** (2003) 095004, doi:[10.1103/PhysRevD.67.095004](https://doi.org/10.1103/PhysRevD.67.095004), arXiv:[hep-ph/0301040](https://arxiv.org/abs/hep-ph/0301040).
- [4] T. Appelquist, H.-C. Cheng, and B. A. Dobrescu, “Bounds on universal extra dimensions”, *Phys. Rev. D* **64** (2001) 035002, doi:[10.1103/PhysRevD.64.035002](https://doi.org/10.1103/PhysRevD.64.035002), arXiv:[hep-ph/0012100v2](https://arxiv.org/abs/hep-ph/0012100v2).
- [5] P. Lodone, “Vector-like quarks in a composite Higgs model”, *JHEP* **12** (2008) 029, doi:[10.1088/1126-6708/2008/12/029](https://doi.org/10.1088/1126-6708/2008/12/029), arXiv:[0806.1472](https://arxiv.org/abs/0806.1472).
- [6] J. Wess and B. Zumino, “Supergauge transformations in four dimensions”, *Nucl. Phys. B* **70** (1974) 39, doi:[10.1016/0550-3213\(74\)90355-1](https://doi.org/10.1016/0550-3213(74)90355-1).

- [7] H. P. Nilles, “Supersymmetry, Supergravity and Particle Physics”, *Phys. Reports* **110** (1984) 1, doi:10.1016/0370-1573(84)90008-5.
- [8] H. E. Haber and G. L. Kane, “The Search for Supersymmetry: Probing Physics Beyond the Standard Model”, *Phys. Reports* **117** (1987) 75, doi:10.1016/0370-1573(85)90051-1.
- [9] R. Barbieri, S. Ferrara, and C. A. Savoy, “Gauge Models with Spontaneously Broken Local Supersymmetry”, *Phys. Lett. B* **119** (1982) 343, doi:10.1016/0370-2693(82)90685-2.
- [10] S. Dawson, E. Eichten, and C. Quigg, “Search for Supersymmetric Particles in Hadron - Hadron Collisions”, *Phys. Rev. D* **31** (1985) 1581, doi:10.1103/PhysRevD.31.1581.
- [11] G. R. Farrar and P. Fayet, “Phenomenology of the production, decay, and detection of new hadronic states associated with supersymmetry”, *Phys. Lett. B* **76** (1978) 575, doi:10.1016/0370-2693(78)90858-4.
- [12] M. Papucci, J. T. Ruderman, and A. Weiler, “Natural SUSY Endures”, *JHEP* **09** (2012) 035, doi:10.1007/JHEP09(2012)035, arXiv:1110.6926.
- [13] C. Brust et al., “SUSY, the Third Generation and the LHC”, *JHEP* **03** (2012) 103, doi:10.1007/JHEP03(2012)103, arXiv:1110.6670.
- [14] CMS Collaboration, “Search for new physics in events with same-sign dileptons and b-tagged jets in pp collisions at $\sqrt{s} = 7$ TeV”, *JHEP* **08** (2012) 110, doi:10.1007/JHEP08(2012)110, arXiv:1205.3933.
- [15] CMS Collaboration, “Search for supersymmetry in hadronic final states using MT2 in pp collisions at $\sqrt{s} = 7$ TeV”, *JHEP* **10** (2012) 018, doi:10.1007/JHEP10(2012)018, arXiv:1207.1798.
- [16] CMS Collaboration, “Search for supersymmetry in events with b-quark jets and missing transverse energy in pp collisions at 7 TeV”, *Phys. Rev. D* **86** (2012) 072010, doi:10.1103/PhysRevD.86.072010, arXiv:1208.4859.
- [17] ATLAS Collaboration, “Search for direct top squark pair production in final states with one isolated lepton, jets, and missing transverse momentum in $\sqrt{s} = 7$ TeV pp collisions using 4.7 fb^{-1} of ATLAS data”, (2012). arXiv:1208.2590. Accepted by *PRL*.
- [18] ATLAS Collaboration, “Search for a supersymmetric partner to the top quark in final states with jets and missing transverse momentum at $\sqrt{s} = 7$ TeV with the ATLAS detector”, (2012). arXiv:1208.1447. Submitted to *PRL*.
- [19] ATLAS Collaboration, “Search for top and bottom squarks from gluino pair production in final states with missing transverse energy and at least three b-jets with the ATLAS detector”, (2012). arXiv:1207.4686. Submitted to *EPJC*.
- [20] ATLAS Collaboration, “Search for supersymmetry in pp collisions at $\sqrt{s} = 7$ TeV in final states with missing transverse momentum and b-jets with the ATLAS detector”, *Phys. Rev. D* **85** (2012) 112006, doi:10.1103/PhysRevD.85.112006, arXiv:1203.6193.
- [21] A. H. Chamseddine, R. Arnowitt, and P. Nath, “Locally Supersymmetric Grand Unification”, *Phys. Rev. Lett.* **49** (1982) 970, doi:10.1103/PhysRevLett.49.970.

- [22] L. Hall, J. Lykken, and S. Weinberg, “Supergravity as the messenger of supersymmetry breaking”, *Phys. Rev. D* **27** (1983) 2359, doi:10.1103/PhysRevD.27.2359.
- [23] N. Arkani-Hamed et al., “MAMBOSET: The Path from LHC Data to the New Standard Model via On-Shell Effective Theories”, (2007). arXiv:hep-ph/0703088.
- [24] D. Daniele Alves et al., “Simplified Models for LHC New Physics Searches”, *J. Phys. G* **39** (2012) 105005, doi:10.1088/0954-3899/39/10/105005, arXiv:1105.2838.
- [25] J. Alwall, P. C. Schuster, and N. Toro, “Simplified Models for a First Characterization of New Physics at the LHC”, *Phys. Rev. D* **79** (2009) 075020, doi:10.1103/PhysRevD.79.075020, arXiv:0810.3921.
- [26] CMS Collaboration, “The CMS experiment at the CERN LHC”, *JINST* **03** (2008) S08004, doi:10.1088/1748-0221/3/08/S08004.
- [27] GEANT4 Collaboration, “GEANT4—a simulation toolkit”, *Nucl. Instrum. Meth. A* **506** (2003) 250, doi:10.1016/S0168-9002(03)01368-8.
- [28] J. Alwall et al., “MadGraph 5: Going Beyond”, *JHEP* **06** (2011) 128, doi:10.1007/JHEP06(2011)128, arXiv:1106.0522.
- [29] T. Sjöstrand, S. Mrenna, and P. Z. Skands, “PYTHIA 6.4 Physics and Manual”, *JHEP* **05** (2006) 026, doi:10.1088/1126-6708/2006/05/026, arXiv:hep-ph/0603175.
- [30] R. Field, “Early LHC underlying event data - findings and surprises”, (2010). arXiv:1010.3558.
- [31] Z. Wąs, “TAUOLA the library for tau lepton decay, and KKMC/KORALB/KORALZ/... status report”, *Nucl. Phys. Proc. Suppl.* **98** (2001) 96, doi:10.1016/S0920-5632(01)01200-2, arXiv:hep-ph/0011305.
- [32] S. Alioli et al., “NLO single-top production matched with shower in POWHEG: s- and t-channel contributions”, *JHEP* **09** (2009) 111, doi:10.1088/1126-6708/2009/09/111, arXiv:0907.4076v2. Erratum-ibid. doi:10.1007/JHEP02(2010)011.
- [33] E. Re, “Single-top Wt-channel production matched with parton showers using the POWHEG method”, *Eur. Phys. J. C* **71** (2011) 1547, doi:10.1140/epjc/s10052-011-1547-z, arXiv:1009.2450.
- [34] B. C. Allanach, “SOFTSUSY: a program for calculating supersymmetric spectra”, *Comput. Phys. Commun.* **143** (2002) 305, doi:10.1016/S0010-4655(01)00460-X, arXiv:hep-ph/0104145.
- [35] CMS Collaboration, “CMS technical design report, volume II: Physics performance”, *J. Phys. G* **34** (2007) 995, doi:10.1088/0954-3899/34/6/S01.
- [36] CMS Collaboration, “Search for new physics in the multijet and missing transverse momentum final state in proton-proton collisions at $\sqrt{s} = 7 \text{ TeV}$ ”, *Phys. Rev. Lett.* **109** (2012) 171803, doi:10.1103/PhysRevLett.109.171803, arXiv:1207.1898.
- [37] S. Abdullin et al., “Fast Simulation of the CMS Detector at the LHC”, in *CHEP 2010*. 2011. *J. Phys.: Conference Series* 331 032049. doi:10.1088/1742-6596/331/3/032049.

- [38] CMS Collaboration, “Performance of CMS muon reconstruction in pp collision events at $\sqrt{s} = 7 \text{ TeV}$ ”, *JINST* **7** (2012) P10002, doi:10.1088/1748-0221/7/10/P10002, arXiv:1206.4071.
- [39] CMS Collaboration, “Electron Reconstruction and Identification at $\sqrt{s} = 7 \text{ TeV}$ ”, CMS Physics Analysis Summary CMS-PAS-EGM-10-004, (2010).
- [40] CMS Collaboration, “Particle–Flow Event Reconstruction in CMS and Performance for Jets, Taus, and E_T^{miss} ”, CMS Physics Analysis Summary CMS-PAS-PFT-09-001, (2009).
- [41] M. Cacciari, G. P. Salam, and G. Soyez, “FastJet user manual”, *Eur. Phys. J. C* **72** (2012) 1896, doi:10.1140/epjc/s10052-012-1896-2, arXiv:1111.6097.
- [42] M. Cacciari, G. P. Salam, and G. Soyez, “The anti- k_t jet clustering algorithm”, *JHEP* **04** (2008) 063, doi:10.1088/1126-6708/2008/04/063.
- [43] CMS Collaboration, “Determination of Jet Energy Calibration and Transverse Momentum Resolution in CMS”, *JINST* **6** (2011) P11002, doi:10.1088/1748-0221/6/11/P11002, arXiv:1107.4277.
- [44] CMS Collaboration, “Identification of b-quark jets at the CMS experiment”, CMS Physics Analysis Summary CMS-PAS-BTV-12-001, (2012).
- [45] CMS Collaboration, “Measuring Electron Efficiencies at CMS with Early Data”, CMS Physics Analysis Summary CMS-PAS-EGM-07-001, (2007).
- [46] V. Pavlunin, “Modeling missing transverse energy in V+jets at CERN LHC”, *Phys. Rev. D* **81** (2010) 035005, doi:10.1103/PhysRevD.81.035005, arXiv:0906.5016.
- [47] J. M. Campbell and R. K. Ellis, “Top-quark processes at NLO in production and decay”, (2012). arXiv:1204.1513.
- [48] M. Botje et al., “The PDF4LHC Working Group Interim Recommendations”, (2011). arXiv:1101.0538.
- [49] A. L. Read, “Presentation of search results: The CL(s) technique”, *J. Phys. G* **28** (2002) 2693, doi:10.1088/0954-3899/28/10/313.
- [50] T. Junk, “Confidence level computation for combining searches with small statistics”, *Nucl. Instrum. Meth. A* **434** (1999) 435, doi:10.1016/S0168-9002(99)00498-2, arXiv:hep-ex/9902006.
- [51] W. Beenakker et al., “Squark and gluino production at hadron colliders”, *Nucl. Phys. B* **492** (1997) 51, doi:10.1016/S0550-3213(97)00084-9, arXiv:hep-ph/9610490.
- [52] A. Kulesza and L. Motyka, “Threshold resummation for squark-antisquark and gluino-pair production at the LHC”, *Phys. Rev. Lett.* **102** (2009) 111802, doi:10.1103/PhysRevLett.102.111802, arXiv:0807.2405.
- [53] A. Kulesza and L. Motyka, “Soft gluon resummation for the production of gluino-gluino and squark-antisquark pairs at the LHC”, *Phys. Rev. D* **80** (2009) 095004, doi:10.1103/PhysRevD.80.095004, arXiv:0905.4749.
- [54] W. Beenakker et al., “Soft-gluon resummation for squark and gluino hadroproduction”, *JHEP* **12** (2009) 041, doi:10.1088/1126-6708/2009/12/041, arXiv:0909.4418.

- [55] W. Beenakker et al., “Squark and Gluino Hadroproduction”, *Int. J. Mod. Phys. A* **26** (2011) 2637, doi:10.1142/S0217751X11053560, arXiv:1105.1110.
- [56] M. Krämer et al., “Supersymmetry production cross sections in pp collisions at $\sqrt{s} = 7 \text{ TeV}$ ”, (2012). arXiv:1206.2892.

A The CMS Collaboration

Yerevan Physics Institute, Yerevan, Armenia

S. Chatrchyan, V. Khachatryan, A.M. Sirunyan, A. Tumasyan

Institut für Hochenergiephysik der OeAW, Wien, Austria

W. Adam, E. Aguilo, T. Bergauer, M. Dragicevic, J. Erö, C. Fabjan¹, M. Friedl, R. Frühwirth¹, V.M. Ghete, J. Hammer, N. Hörmann, J. Hrubec, M. Jeitler¹, W. Kiesenhofer, V. Knünz, M. Krammer¹, I. Krätschmer, D. Liko, I. Mikulec, M. Pernicka[†], B. Rahbaran, C. Rohringer, H. Rohringer, R. Schöfbeck, J. Strauss, A. Taurok, W. Waltenberger, G. Walzel, E. Widl, C.-E. Wulz¹

National Centre for Particle and High Energy Physics, Minsk, Belarus

V. Mossolov, N. Shumeiko, J. Suarez Gonzalez

Universiteit Antwerpen, Antwerpen, Belgium

M. Bansal, S. Bansal, T. Cornelis, E.A. De Wolf, X. Janssen, S. Luyckx, L. Mucibello, S. Ochesanu, B. Roland, R. Rougny, M. Selvaggi, Z. Staykova, H. Van Haevermaet, P. Van Mechelen, N. Van Remortel, A. Van Spilbeeck

Vrije Universiteit Brussel, Brussel, Belgium

F. Blekman, S. Blyweert, J. D'Hondt, R. Gonzalez Suarez, A. Kalogeropoulos, M. Maes, A. Olbrechts, W. Van Doninck, P. Van Mulders, G.P. Van Onsem, I. Villella

Université Libre de Bruxelles, Bruxelles, Belgium

B. Clerbaux, G. De Lentdecker, V. Dero, A.P.R. Gay, T. Hreus, A. Léonard, P.E. Marage, A. Mohammadi, T. Reis, L. Thomas, G. Vander Marcken, C. Vander Velde, P. Vanlaer, J. Wang

Ghent University, Ghent, Belgium

V. Adler, K. Beernaert, A. Cimmino, S. Costantini, G. Garcia, M. Grunewald, B. Klein, J. Lellouch, A. Marinov, J. Mccartin, A.A. Ocampo Rios, D. Ryckbosch, N. Strobbe, F. Thyssen, M. Tytgat, P. Verwilligen, S. Walsh, E. Yazgan, N. Zaganidis

Université Catholique de Louvain, Louvain-la-Neuve, Belgium

S. Basegmez, G. Bruno, R. Castello, L. Ceard, C. Delaere, T. du Pree, D. Favart, L. Forthomme, A. Giannanco², J. Hollar, V. Lemaitre, J. Liao, O. Militaru, C. Nuttens, D. Pagano, A. Pin, K. Piotrkowski, N. Schul, J.M. Vizan Garcia

Université de Mons, Mons, Belgium

N. Belyi, T. Caebergs, E. Daubie, G.H. Hammad

Centro Brasileiro de Pesquisas Fisicas, Rio de Janeiro, Brazil

G.A. Alves, M. Correa Martins Junior, D. De Jesus Damiao, T. Martins, M.E. Pol, M.H.G. Souza

Universidade do Estado do Rio de Janeiro, Rio de Janeiro, Brazil

W.L. Aldá Júnior, W. Carvalho, A. Custódio, E.M. Da Costa, C. De Oliveira Martins, S. Fonseca De Souza, D. Matos Figueiredo, L. Mundim, H. Nogima, V. Oguri, W.L. Prado Da Silva, A. Santoro, L. Soares Jorge, A. Sznajder

Instituto de Fisica Teorica ^a, Universidade Estadual Paulista ^b, Sao Paulo, Brazil

T.S. Anjos^{b,3}, C.A. Bernardes^{b,3}, F.A. Dias^{a,4}, T.R. Fernandez Perez Tomei^a, E.M. Gregores^{b,3}, C. Lagana^a, F. Marinho^a, P.G. Mercadante^{b,3}, S.F. Novaes^a, Sandra S. Padula^a

Institute for Nuclear Research and Nuclear Energy, Sofia, Bulgaria

V. Genchev⁵, P. Iaydjiev⁵, S. Piperov, M. Rodozov, S. Stoykova, G. Sultanov, V. Tcholakov, R. Trayanov, M. Vutova

University of Sofia, Sofia, Bulgaria

A. Dimitrov, R. Hadjiiska, V. Kozuharov, L. Litov, B. Pavlov, P. Petkov

Institute of High Energy Physics, Beijing, China

J.G. Bian, G.M. Chen, H.S. Chen, C.H. Jiang, D. Liang, S. Liang, X. Meng, J. Tao, J. Wang, X. Wang, Z. Wang, H. Xiao, M. Xu, J. Zang, Z. Zhang

State Key Lab. of Nucl. Phys. and Tech., Peking University, Beijing, China

C. Asawatangtrakuldee, Y. Ban, Y. Guo, W. Li, S. Liu, Y. Mao, S.J. Qian, H. Teng, D. Wang, L. Zhang, W. Zou

Universidad de Los Andes, Bogota, Colombia

C. Avila, J.P. Gomez, B. Gomez Moreno, A.F. Osorio Oliveros, J.C. Sanabria

Technical University of Split, Split, Croatia

N. Godinovic, D. Lelas, R. Plestina⁶, D. Polic, I. Puljak⁵

University of Split, Split, Croatia

Z. Antunovic, M. Kovac

Institute Rudjer Boskovic, Zagreb, Croatia

V. Brigljevic, S. Duric, K. Kadija, J. Luetic, S. Morovic

University of Cyprus, Nicosia, Cyprus

A. Attikis, M. Galanti, G. Mavromanolakis, J. Mousa, C. Nicolaou, F. Ptochos, P.A. Razis

Charles University, Prague, Czech Republic

M. Finger, M. Finger Jr.

Academy of Scientific Research and Technology of the Arab Republic of Egypt, Egyptian Network of High Energy Physics, Cairo, Egypt

Y. Assran⁷, S. Elgammal⁸, A. Ellithi Kamel⁹, M.A. Mahmoud¹⁰, A. Radi^{11,12}

National Institute of Chemical Physics and Biophysics, Tallinn, Estonia

M. Kadastik, M. Müntel, M. Raidal, L. Rebane, A. Tiko

Department of Physics, University of Helsinki, Helsinki, Finland

P. Eerola, G. Fedi, M. Voutilainen

Helsinki Institute of Physics, Helsinki, Finland

J. Hätkönen, A. Heikkinen, V. Karimäki, R. Kinnunen, M.J. Kortelainen, T. Lampén, K. Lassila-Perini, S. Lehti, T. Lindén, P. Luukka, T. Mäenpää, T. Peltola, E. Tuominen, J. Tuominiemi, E. Tuovinen, D. Ungaro, L. Wendland

Lappeenranta University of Technology, Lappeenranta, Finland

K. Banzuzi, A. Karjalainen, A. Korpela, T. Tuuva

DSM/IRFU, CEA/Saclay, Gif-sur-Yvette, France

M. Besancon, S. Choudhury, M. Dejardin, D. Denegri, B. Fabbro, J.L. Faure, F. Ferri, S. Ganjour, A. Givernaud, P. Gras, G. Hamel de Monchenault, P. Jarry, E. Locci, J. Malcles, L. Millischer, A. Nayak, J. Rander, A. Rosowsky, I. Shreyber, M. Titov

Laboratoire Leprince-Ringuet, Ecole Polytechnique, IN2P3-CNRS, Palaiseau, France

S. Baffioni, F. Beaudette, L. Benhabib, L. Bianchini, M. Bluj¹³, C. Broutin, P. Busson, C. Charlot, N. Daci, T. Dahms, M. Dalchenko, L. Dobrzynski, R. Granier de Cassagnac, M. Haguenauer, P. Miné, C. Mironov, I.N. Naranjo, M. Nguyen, C. Ochando, P. Paganini, D. Sabes, R. Salerno, Y. Sirois, C. Veelken, A. Zabi

Institut Pluridisciplinaire Hubert Curien, Université de Strasbourg, Université de Haute Alsace Mulhouse, CNRS/IN2P3, Strasbourg, France

J.-L. Agram¹⁴, J. Andrea, D. Bloch, D. Bodin, J.-M. Brom, M. Cardaci, E.C. Chabert, C. Collard, E. Conte¹⁴, F. Drouhin¹⁴, C. Ferro, J.-C. Fontaine¹⁴, D. Gelé, U. Goerlach, P. Juillot, A.-C. Le Bihan, P. Van Hove

Centre de Calcul de l’Institut National de Physique Nucléaire et de Physique des Particules, CNRS/IN2P3, Villeurbanne, France, Villeurbanne, France

F. Fassi, D. Mercier

Université de Lyon, Université Claude Bernard Lyon 1, CNRS-IN2P3, Institut de Physique Nucléaire de Lyon, Villeurbanne, France

S. Beauceron, N. Beaupere, O. Bondu, G. Boudoul, J. Chasserat, R. Chierici⁵, D. Contardo, P. Depasse, H. El Mamouni, J. Fay, S. Gascon, M. Gouzevitch, B. Ille, T. Kurca, M. Lethuillier, L. Mirabito, S. Perries, L. Sgandurra, V. Sordini, Y. Tschudi, P. Verdier, S. Viret

Institute of High Energy Physics and Informatization, Tbilisi State University, Tbilisi, Georgia

Z. Tsamalaidze¹⁵

RWTH Aachen University, I. Physikalisches Institut, Aachen, Germany

G. Anagnostou, C. Autermann, S. Beranek, M. Edelhoff, L. Feld, N. Heracleous, O. Hindrichs, R. Jussen, K. Klein, J. Merz, A. Ostapchuk, A. Perieanu, F. Raupach, J. Sammet, S. Schael, D. Sprenger, H. Weber, B. Wittmer, V. Zhukov¹⁶

RWTH Aachen University, III. Physikalisches Institut A, Aachen, Germany

M. Ata, J. Caudron, E. Dietz-Laursonn, D. Duchardt, M. Erdmann, R. Fischer, A. Güth, T. Hebbeker, C. Heidemann, K. Hoepfner, D. Klingebiel, P. Kreuzer, M. Merschmeyer, A. Meyer, M. Olszewski, P. Papacz, H. Pieta, H. Reithler, S.A. Schmitz, L. Sonnenschein, J. Steggemann, D. Teyssier, M. Weber

RWTH Aachen University, III. Physikalisches Institut B, Aachen, Germany

M. Bontenackels, V. Cherepanov, Y. Erdogan, G. Flügge, H. Geenen, M. Geisler, W. Haj Ahmad, F. Hoehle, B. Kargoll, T. Kress, Y. Kuessel, J. Lingemann⁵, A. Nowack, L. Perchalla, O. Pooth, P. Sauerland, A. Stahl

Deutsches Elektronen-Synchrotron, Hamburg, Germany

M. Aldaya Martin, J. Behr, W. Behrenhoff, U. Behrens, M. Bergholz¹⁷, A. Bethani, K. Borras, A. Burgmeier, A. Cakir, L. Calligaris, A. Campbell, E. Castro, F. Costanza, D. Dammann, C. Diez Pardos, G. Eckstein, D. Eckstein, G. Flucke, A. Geiser, I. Glushkov, P. Gunnellini, S. Habib, J. Hauk, G. Hellwig, D. Horton, H. Jung, M. Kasemann, P. Katsas, C. Kleinwort, H. Kluge, A. Knutsson, M. Krämer, D. Krücker, E. Kuznetsova, W. Lange, W. Lohmann¹⁷, B. Lutz, R. Mankel, I. Marfin, M. Marienfeld, I.-A. Melzer-Pellmann, A.B. Meyer, J. Mnich, A. Mussgiller, S. Naumann-Emme, O. Novgorodova, J. Olzem, H. Perrey, A. Petrukhin, D. Pitzl, A. Raspereza, P.M. Ribeiro Cipriano, C. Riedl, E. Ron, M. Rosin, J. Salfeld-Nebgen, R. Schmidt¹⁷, T. Schoerner-Sadenius, N. Sen, A. Spiridonov, M. Stein, R. Walsh, C. Wissing

University of Hamburg, Hamburg, Germany

V. Blobel, J. Draeger, H. Enderle, J. Erfle, U. Gebbert, M. Görner, T. Hermanns, R.S. Höing, K. Kaschube, G. Kaussen, H. Kirschenmann, R. Klanner, J. Lange, B. Mura, F. Nowak, T. Peiffer, N. Pietsch, D. Rathjens, C. Sander, H. Schettler, P. Schleper, E. Schlieckau, A. Schmidt, M. Schröder, T. Schum, M. Seidel, V. Sola, H. Stadie, G. Steinbrück, J. Thomsen, L. Vanelderden

Institut für Experimentelle Kernphysik, Karlsruhe, Germany

C. Barth, J. Berger, C. Böser, T. Chwalek, W. De Boer, A. Descroix, A. Dierlamm, M. Feindt, M. Guthoff⁵, C. Hackstein, F. Hartmann, T. Hauth⁵, M. Heinrich, H. Held, K.H. Hoffmann, U. Husemann, I. Katkov¹⁶, J.R. Komaragiri, P. Lobelle Pardo, D. Martschei, S. Mueller, Th. Müller, M. Niegel, A. Nürnberg, O. Oberst, A. Oehler, J. Ott, G. Quast, K. Rabbertz, F. Ratnikov, N. Ratnikova, S. Röcker, F.-P. Schilling, G. Schott, H.J. Simonis, F.M. Stober, D. Troendle, R. Ulrich, J. Wagner-Kuhr, S. Wayand, T. Weiler, M. Zeise

Institute of Nuclear Physics "Demokritos", Aghia Paraskevi, Greece

G. Daskalakis, T. Geralis, S. Kesisoglou, A. Kyriakis, D. Loukas, I. Manolakos, A. Markou, C. Markou, C. Mavrommatis, E. Ntomari

University of Athens, Athens, Greece

L. Gouskos, T.J. Mertzimekis, A. Panagiotou, N. Saoulidou

University of Ioánnina, Ioánnina, Greece

I. Evangelou, C. Foudas, P. Kokkas, N. Manthos, I. Papadopoulos, V. Patras

KFKI Research Institute for Particle and Nuclear Physics, Budapest, Hungary

G. Bencze, C. Hajdu, P. Hidas, D. Horvath¹⁸, F. Sikler, V. Veszpremi, G. Vesztergombi¹⁹

Institute of Nuclear Research ATOMKI, Debrecen, Hungary

N. Beni, S. Czellar, J. Molnar, J. Palinkas, Z. Szillasi

University of Debrecen, Debrecen, Hungary

J. Karancsi, P. Raics, Z.L. Trocsanyi, B. Ujvari

Panjab University, Chandigarh, India

S.B. Beri, V. Bhatnagar, N. Dhingra, R. Gupta, M. Kaur, M.Z. Mehta, N. Nishu, L.K. Saini, A. Sharma, J.B. Singh

University of Delhi, Delhi, India

Ashok Kumar, Arun Kumar, S. Ahuja, A. Bhardwaj, B.C. Choudhary, S. Malhotra, M. Naimuddin, K. Ranjan, V. Sharma, R.K. Shrivpuri

Saha Institute of Nuclear Physics, Kolkata, India

S. Banerjee, S. Bhattacharya, S. Dutta, B. Gomber, Sa. Jain, Sh. Jain, R. Khurana, S. Sarkar, M. Sharan

Bhabha Atomic Research Centre, Mumbai, India

A. Abdulsalam, R.K. Choudhury, D. Dutta, S. Kailas, V. Kumar, P. Mehta, A.K. Mohanty⁵, L.M. Pant, P. Shukla

Tata Institute of Fundamental Research - EHEP, Mumbai, India

T. Aziz, S. Ganguly, M. Guchait²⁰, M. Maity²¹, G. Majumder, K. Mazumdar, G.B. Mohanty, B. Parida, K. Sudhakar, N. Wickramage

Tata Institute of Fundamental Research - HEGR, Mumbai, India

S. Banerjee, S. Dugad

Institute for Research in Fundamental Sciences (IPM), Tehran, Iran

H. Arfaei²², H. Bakhshiansohi, S.M. Etesami²³, A. Fahim²², M. Hashemi, H. Hesari, A. Jafari, M. Khakzad, M. Mohammadi Najafabadi, S. Pakhtinat Mehdiabadi, B. Safarzadeh²⁴, M. Zeinali

INFN Sezione di Bari ^a, Università di Bari ^b, Politecnico di Bari ^c, Bari, Italy

M. Abbrescia^{a,b}, L. Barbone^{a,b}, C. Calabria^{a,b,5}, S.S. Chhibra^{a,b}, A. Colaleo^a, D. Creanza^{a,c},

N. De Filippis^{a,c,5}, M. De Palma^{a,b}, L. Fiore^a, G. Iaselli^{a,c}, L. Lusito^{a,b}, G. Maggi^{a,c}, M. Maggi^a, B. Marangelli^{a,b}, S. My^{a,c}, S. Nuzzo^{a,b}, N. Pacifico^{a,b}, A. Pompili^{a,b}, G. Pugliese^{a,c}, G. Selvaggi^{a,b}, L. Silvestris^a, G. Singh^{a,b}, R. Venditti^{a,b}, G. Zito^a

INFN Sezione di Bologna ^a, Università di Bologna ^b, Bologna, Italy

G. Abbiendi^a, A.C. Benvenuti^a, D. Bonacorsi^{a,b}, S. Braibant-Giacomelli^{a,b}, L. Brigliadori^{a,b}, P. Capiluppi^{a,b}, A. Castro^{a,b}, F.R. Cavallo^a, M. Cuffiani^{a,b}, G.M. Dallavalle^a, F. Fabbri^a, A. Fanfani^{a,b}, D. Fasanella^{a,b,5}, P. Giacomelli^a, C. Grandi^a, L. Guiducci^{a,b}, S. Marcellini^a, G. Masetti^a, M. Meneghelli^{a,b,5}, A. Montanari^a, F.L. Navarria^{a,b}, F. Odorici^a, A. Perrotta^a, F. Primavera^{a,b}, A.M. Rossi^{a,b}, T. Rovelli^{a,b}, G.P. Siroli^{a,b}, R. Travaglini^{a,b}

INFN Sezione di Catania ^a, Università di Catania ^b, Catania, Italy

S. Albergo^{a,b}, G. Cappello^{a,b}, M. Chiorboli^{a,b}, S. Costa^{a,b}, R. Potenza^{a,b}, A. Tricomi^{a,b}, C. Tuve^{a,b}

INFN Sezione di Firenze ^a, Università di Firenze ^b, Firenze, Italy

G. Barbagli^a, V. Ciulli^{a,b}, C. Civinini^a, R. D'Alessandro^{a,b}, E. Focardi^{a,b}, S. Frosali^{a,b}, E. Gallo^a, S. Gonzi^{a,b}, M. Meschini^a, S. Paoletti^a, G. Sguazzoni^a, A. Tropiano^{a,b}

INFN Laboratori Nazionali di Frascati, Frascati, Italy

L. Benussi, S. Bianco, S. Colafranceschi²⁵, F. Fabbri, D. Piccolo

INFN Sezione di Genova ^a, Università di Genova ^b, Genova, Italy

P. Fabbricatore^a, R. Musenich^a, S. Tosi^{a,b}

INFN Sezione di Milano-Bicocca ^a, Università di Milano-Bicocca ^b, Milano, Italy

A. Benaglia^{a,b}, F. De Guio^{a,b}, L. Di Matteo^{a,b,5}, S. Fiorendi^{a,b}, S. Gennai^{a,5}, A. Ghezzi^{a,b}, S. Malvezzi^a, R.A. Manzoni^{a,b}, A. Martelli^{a,b}, A. Massironi^{a,b,5}, D. Menasce^a, L. Moroni^a, M. Paganoni^{a,b}, D. Pedrini^a, S. Ragazzi^{a,b}, N. Redaelli^a, S. Sala^a, T. Tabarelli de Fatis^{a,b}

INFN Sezione di Napoli ^a, Università di Napoli "Federico II" ^b, Napoli, Italy

S. Buontempo^a, C.A. Carrillo Montoya^a, N. Cavallo^{a,26}, A. De Cosa^{a,b,5}, O. Dogangun^{a,b}, F. Fabozzi^{a,26}, A.O.M. Iorio^{a,b}, L. Lista^a, S. Meola^{a,27}, M. Merola^{a,b}, P. Paolucci^{a,5}

INFN Sezione di Padova ^a, Università di Padova ^b, Università di Trento (Trento) ^c, Padova, Italy

P. Azzi^a, N. Bacchetta^{a,5}, P. Bellan^{a,b}, D. Bisello^{a,b}, A. Branca^{a,b,5}, R. Carlin^{a,b}, P. Checchia^a, T. Dorigo^a, U. Dosselli^a, F. Gasparini^{a,b}, U. Gasparini^{a,b}, A. Gozzelino^a, K. Kanishchev^{a,c}, S. Lacaprara^a, I. Lazzizzera^{a,c}, M. Margoni^{a,b}, A.T. Meneguzzo^{a,b}, M. Nespolo^{a,5}, J. Pazzini^{a,b}, P. Ronchese^{a,b}, F. Simonetto^{a,b}, E. Torassa^a, S. Vanini^{a,b}, P. Zotto^{a,b}, G. Zumerle^{a,b}

INFN Sezione di Pavia ^a, Università di Pavia ^b, Pavia, Italy

M. Gabusi^{a,b}, S.P. Ratti^{a,b}, C. Riccardi^{a,b}, P. Torre^{a,b}, P. Vitulo^{a,b}

INFN Sezione di Perugia ^a, Università di Perugia ^b, Perugia, Italy

M. Biasini^{a,b}, G.M. Bilei^a, L. Fanò^{a,b}, P. Lariccia^{a,b}, G. Mantovani^{a,b}, M. Menichelli^a, A. Nappi^{a,b†}, F. Romeo^{a,b}, A. Saha^a, A. Santocchia^{a,b}, A. Spiezia^{a,b}, S. Taroni^{a,b}

INFN Sezione di Pisa ^a, Università di Pisa ^b, Scuola Normale Superiore di Pisa ^c, Pisa, Italy

P. Azzurri^{a,c}, G. Bagliesi^a, J. Bernardini^a, T. Boccali^a, G. Broccolo^{a,c}, R. Castaldi^a, R.T. D'Agnolo^{a,c,5}, R. Dell'Orso^a, F. Fiori^{a,b,5}, L. Foà^{a,c}, A. Giassi^a, A. Kraan^a, F. Ligabue^{a,c}, T. Lomtadze^a, L. Martini^{a,28}, A. Messineo^{a,b}, F. Palla^a, A. Rizzi^{a,b}, A.T. Serban^{a,29}, P. Spagnolo^a, P. Squillaciotti^{a,5}, R. Tenchini^a, G. Tonelli^{a,b}, A. Venturi^a, P.G. Verdini^a

INFN Sezione di Roma ^a, Università di Roma ^b, Roma, Italy

L. Barone^{a,b}, F. Cavallari^a, D. Del Re^{a,b}, M. Diemoz^a, C. Fanelli^{a,b}, M. Grassi^{a,b,5}, E. Longo^{a,b},

P. Meridiani^{a,5}, F. Micheli^{a,b}, S. Nourbakhsh^{a,b}, G. Organtini^{a,b}, R. Paramatti^a, S. Rahatlou^{a,b}, M. Sigamani^a, L. Soffi^{a,b}

INFN Sezione di Torino ^a, Università di Torino ^b, Università del Piemonte Orientale (Novara) ^c, Torino, Italy

N. Amapane^{a,b}, R. Arcidiacono^{a,c}, S. Argiro^{a,b}, M. Arneodo^{a,c}, C. Biino^a, N. Cartiglia^a, M. Costa^{a,b}, N. Demaria^a, C. Mariotti^{a,5}, S. Maselli^a, E. Migliore^{a,b}, V. Monaco^{a,b}, M. Musich^{a,5}, M.M. Obertino^{a,c}, N. Pastrone^a, M. Pelliccioni^a, A. Potenza^{a,b}, A. Romero^{a,b}, M. Ruspa^{a,c}, R. Sacchi^{a,b}, A. Solano^{a,b}, A. Staiano^a, A. Vilela Pereira^a

INFN Sezione di Trieste ^a, Università di Trieste ^b, Trieste, Italy

S. Belforte^a, V. Candelise^{a,b}, M. Casarsa^a, F. Cossutti^a, G. Della Ricca^{a,b}, B. Gobbo^a, M. Marone^{a,b,5}, D. Montanino^{a,b,5}, A. Penzo^a, A. Schizzi^{a,b}

Kangwon National University, Chunchon, Korea

S.G. Heo, T.Y. Kim, S.K. Nam

Kyungpook National University, Daegu, Korea

S. Chang, D.H. Kim, G.N. Kim, D.J. Kong, H. Park, S.R. Ro, D.C. Son, T. Son

Chonnam National University, Institute for Universe and Elementary Particles, Kwangju, Korea

J.Y. Kim, Zero J. Kim, S. Song

Korea University, Seoul, Korea

S. Choi, D. Gyun, B. Hong, M. Jo, H. Kim, T.J. Kim, K.S. Lee, D.H. Moon, S.K. Park

University of Seoul, Seoul, Korea

M. Choi, J.H. Kim, C. Park, I.C. Park, S. Park, G. Ryu

Sungkyunkwan University, Suwon, Korea

Y. Cho, Y. Choi, Y.K. Choi, J. Goh, M.S. Kim, E. Kwon, B. Lee, J. Lee, S. Lee, H. Seo, I. Yu

Vilnius University, Vilnius, Lithuania

M.J. Bilinskas, I. Grigelionis, M. Janulis, A. Juodagalvis

Centro de Investigacion y de Estudios Avanzados del IPN, Mexico City, Mexico

H. Castilla-Valdez, E. De La Cruz-Burelo, I. Heredia-de La Cruz, R. Lopez-Fernandez, R. Magaña Villalba, J. Martínez-Ortega, A. Sánchez-Hernández, L.M. Villasenor-Cendejas

Universidad Iberoamericana, Mexico City, Mexico

S. Carrillo Moreno, F. Vazquez Valencia

Benemerita Universidad Autonoma de Puebla, Puebla, Mexico

H.A. Salazar Ibarguen

Universidad Autónoma de San Luis Potosí, San Luis Potosí, Mexico

E. Casimiro Linares, A. Morelos Pineda, M.A. Reyes-Santos

University of Auckland, Auckland, New Zealand

D. Kofcheck

University of Canterbury, Christchurch, New Zealand

A.J. Bell, P.H. Butler, R. Doesburg, S. Reucroft, H. Silverwood

National Centre for Physics, Quaid-I-Azam University, Islamabad, Pakistan

M. Ahmad, M.H. Ansari, M.I. Asghar, H.R. Hoorani, S. Khalid, W.A. Khan, T. Khurshid, S. Qazi, M.A. Shah, M. Shoail

National Centre for Nuclear Research, Swierk, Poland

H. Bialkowska, B. Boimska, T. Frueboes, R. Gokieli, M. Górska, M. Kazana, K. Nawrocki, K. Romanowska-Rybinska, M. Szleper, G. Wrochna, P. Zalewski

Institute of Experimental Physics, Faculty of Physics, University of Warsaw, Warsaw, Poland

G. Brona, K. Bunkowski, M. Cwiok, W. Dominik, K. Doroba, A. Kalinowski, M. Konecki, J. Krolikowski

Laboratório de Instrumentação e Física Experimental de Partículas, Lisboa, Portugal

N. Almeida, P. Bargassa, A. David, P. Faccioli, P.G. Ferreira Parracho, M. Gallinaro, J. Seixas, J. Varela, P. Vischia

Joint Institute for Nuclear Research, Dubna, Russia

I. Belotelov, P. Bunin, M. Gavrilenko, I. Golutvin, V. Karjavin, V. Konoplyanikov, G. Kozlov, A. Lanev, A. Malakhov, P. Moisenz, V. Palichik, V. Perelygin, M. Savina, S. Shmatov, V. Smirnov, A. Volodko, A. Zarubin

Petersburg Nuclear Physics Institute, Gatchina (St. Petersburg), Russia

S. Evstukhin, V. Golovtsov, Y. Ivanov, V. Kim, P. Levchenko, V. Murzin, V. Oreshkin, I. Smirnov, V. Sulimov, L. Uvarov, S. Vavilov, A. Vorobyev, An. Vorobyev

Institute for Nuclear Research, Moscow, Russia

Yu. Andreev, A. Dermenev, S. Gninenko, N. Golubev, M. Kirsanov, N. Krasnikov, V. Matveev, A. Pashenkov, D. Tlisov, A. Toropin

Institute for Theoretical and Experimental Physics, Moscow, Russia

V. Epshteyn, M. Erofeeva, V. Gavrilov, M. Kossov, N. Lychkovskaya, V. Popov, G. Safronov, S. Semenov, V. Stolin, E. Vlasov, A. Zhokin

Moscow State University, Moscow, Russia

A. Belyaev, E. Boos, M. Dubinin⁴, L. Dudko, A. Ershov, A. Gribushin, V. Klyukhin, O. Kodolova, I. Loktin, A. Markina, S. Obraztsov, M. Perfilov, S. Petrushanko, A. Popov, L. Sarycheva[†], V. Savrin, A. Snigirev

P.N. Lebedev Physical Institute, Moscow, Russia

V. Andreev, M. Azarkin, I. Dremin, M. Kirakosyan, A. Leonidov, G. Mesyats, S.V. Rusakov, A. Vinogradov

State Research Center of Russian Federation, Institute for High Energy Physics, Protvino, Russia

I. Azhgirey, I. Bayshev, S. Bitioukov, V. Grishin⁵, V. Kachanov, D. Konstantinov, V. Krychkine, V. Petrov, R. Ryutin, A. Sobol, L. Tourtchanovitch, S. Troshin, N. Tyurin, A. Uzunian, A. Volkov

University of Belgrade, Faculty of Physics and Vinca Institute of Nuclear Sciences, Belgrade, Serbia

P. Adzic³⁰, M. Djordjevic, M. Ekmedzic, D. Krpic³⁰, J. Milosevic

Centro de Investigaciones Energéticas Medioambientales y Tecnológicas (CIEMAT), Madrid, Spain

M. Aguilar-Benitez, J. Alcaraz Maestre, P. Arce, C. Battilana, E. Calvo, M. Cerrada, M. Chamizo Llatas, N. Colino, B. De La Cruz, A. Delgado Peris, D. Domínguez Vázquez, C. Fernandez

Bedoya, J.P. Fernández Ramos, A. Ferrando, J. Flix, M.C. Fouz, P. Garcia-Abia, O. Gonzalez Lopez, S. Goy Lopez, J.M. Hernandez, M.I. Josa, G. Merino, J. Puerta Pelayo, A. Quintario Olmeda, I. Redondo, L. Romero, J. Santaolalla, M.S. Soares, C. Willmott

Universidad Autónoma de Madrid, Madrid, Spain

C. Albajar, G. Codispoti, J.F. de Trocóniz

Universidad de Oviedo, Oviedo, Spain

H. Brun, J. Cuevas, J. Fernandez Menendez, S. Folgueras, I. Gonzalez Caballero, L. Lloret Iglesias, J. Piedra Gomez

Instituto de Física de Cantabria (IFCA), CSIC-Universidad de Cantabria, Santander, Spain

J.A. Brochero Cifuentes, I.J. Cabrillo, A. Calderon, S.H. Chuang, J. Duarte Campderros, M. Felcini³¹, M. Fernandez, G. Gomez, J. Gonzalez Sanchez, A. Graziano, C. Jorda, A. Lopez Virto, J. Marco, R. Marco, C. Martinez Rivero, F. Matorras, F.J. Munoz Sanchez, T. Rodrigo, A.Y. Rodríguez-Marrero, A. Ruiz-Jimeno, L. Scodellaro, I. Vila, R. Vilar Cortabitarte

CERN, European Organization for Nuclear Research, Geneva, Switzerland

D. Abbaneo, E. Auffray, G. Auzinger, M. Bachtis, P. Baillon, A.H. Ball, D. Barney, J.F. Benitez, C. Bernet⁶, G. Bianchi, P. Bloch, A. Bocci, A. Bonato, C. Botta, H. Breuker, T. Camporesi, G. Cerminara, T. Christiansen, J.A. Coarasa Perez, D. D'Enterria, A. Dabrowski, A. De Roeck, S. Di Guida, M. Dobson, N. Dupont-Sagorin, A. Elliott-Peisert, B. Frisch, W. Funk, G. Georgiou, M. Giffels, D. Gigi, K. Gill, D. Giordano, M. Girone, M. Giunta, F. Gleje, R. Gomez-Reino Garrido, P. Govoni, S. Gowdy, R. Guida, M. Hansen, P. Harris, C. Hartl, J. Harvey, B. Hegner, A. Hinzmann, V. Innocente, P. Janot, K. Kaadze, E. Karavakis, K. Kousouris, P. Lecoq, Y.-J. Lee, P. Lenzi, C. Lourenço, N. Magini, T. Mäki, M. Malberti, L. Malgeri, M. Mannelli, L. Masetti, F. Meijers, S. Mersi, E. Meschi, R. Moser, M.U. Mozer, M. Mulders, P. Musella, E. Nesvold, T. Orimoto, L. Orsini, E. Palencia Cortezon, E. Perez, L. Perrozzi, A. Petrilli, A. Pfeiffer, M. Pierini, M. Pimiä, D. Piparo, G. Polese, L. Quertenmont, A. Racz, W. Reece, J. Rodrigues Antunes, G. Rolandi³², C. Rovelli³³, M. Rovere, H. Sakulin, F. Santanastasio, C. Schäfer, C. Schwick, I. Segoni, S. Sekmen, A. Sharma, P. Siegrist, P. Silva, M. Simon, P. Sphicas³⁴, D. Spiga, A. Tsirou, G.I. Veres¹⁹, J.R. Vlimant, H.K. Wöhri, S.D. Worm³⁵, W.D. Zeuner

Paul Scherrer Institut, Villigen, Switzerland

W. Bertl, K. Deiters, W. Erdmann, K. Gabathuler, R. Horisberger, Q. Ingram, H.C. Kaestli, S. König, D. Kotlinski, U. Langenegger, F. Meier, D. Renker, T. Rohe, J. Sibille³⁶

Institute for Particle Physics, ETH Zurich, Zurich, Switzerland

L. Bäni, P. Bortignon, M.A. Buchmann, B. Casal, N. Chanon, A. Deisher, G. Dissertori, M. Dittmar, M. Donegà, M. Dünser, J. Eugster, K. Freudenreich, C. Grab, D. Hits, P. Lecomte, W. Lustermann, A.C. Marini, P. Martinez Ruiz del Arbol, N. Mohr, F. Moortgat, C. Nägeli³⁷, P. Nef, F. Nessi-Tedaldi, F. Pandolfi, L. Pape, F. Pauss, M. Peruzzi, F.J. Ronga, M. Rossini, L. Sala, A.K. Sanchez, A. Starodumov³⁸, B. Stieger, M. Takahashi, L. Tauscher[†], A. Thea, K. Theofilatos, D. Treille, C. Urscheler, R. Wallny, H.A. Weber, L. Wehrli

Universität Zürich, Zurich, Switzerland

C. Amsler³⁹, V. Chiochia, S. De Visscher, C. Favaro, M. Ivova Rikova, B. Millan Mejias, P. Otiougova, P. Robmann, H. Snoek, S. Tupputi, M. Verzetti

National Central University, Chung-Li, Taiwan

Y.H. Chang, K.H. Chen, C.M. Kuo, S.W. Li, W. Lin, Z.K. Liu, Y.J. Lu, D. Mekterovic, A.P. Singh, R. Volpe, S.S. Yu

National Taiwan University (NTU), Taipei, Taiwan

P. Bartalini, P. Chang, Y.H. Chang, Y.W. Chang, Y. Chao, K.F. Chen, C. Dietz, U. Grundler, W.-S. Hou, Y. Hsiung, K.Y. Kao, Y.J. Lei, R.-S. Lu, D. Majumder, E. Petrakou, X. Shi, J.G. Shiu, Y.M. Tzeng, X. Wan, M. Wang

Chulalongkorn University, Bangkok, Thailand

B. Asavapibhop, N. Srimanobhas

Cukurova University, Adana, Turkey

A. Adiguzel, M.N. Bakirci⁴⁰, S. Cerci⁴¹, C. Dozen, I. Dumanoglu, E. Eskut, S. Grgis, G. Gokbulut, E. Gurpinar, I. Hos, E.E. Kangal, T. Karaman, G. Karapinar⁴², A. Kayis Topaksu, G. Onengut, K. Ozdemir, S. Ozturk⁴³, A. Polatoz, K. Sogut⁴⁴, D. Sunar Cerci⁴¹, B. Tali⁴¹, H. Topakli⁴⁰, L.N. Vergili, M. Vergili

Middle East Technical University, Physics Department, Ankara, Turkey

I.V. Akin, T. Aliev, B. Bilin, S. Bilmis, M. Deniz, H. Gamsizkan, A.M. Guler, K. Ocalan, A. Ozpineci, M. Serin, R. Sever, U.E. Surat, M. Yalvac, E. Yildirim, M. Zeyrek

Bogazici University, Istanbul, Turkey

E. Grlmez, B. Isildak⁴⁵, M. Kaya⁴⁶, O. Kaya⁴⁶, S. Ozkorucuklu⁴⁷, N. Sonmez⁴⁸

Istanbul Technical University, Istanbul, Turkey

K. Cankocak

National Scientific Center, Kharkov Institute of Physics and Technology, Kharkov, Ukraine

L. Levchuk

University of Bristol, Bristol, United Kingdom

F. Bostock, J.J. Brooke, E. Clement, D. Cussans, H. Flacher, R. Frazier, J. Goldstein, M. Grimes, G.P. Heath, H.F. Heath, L. Kreczko, S. Metson, D.M. Newbold³⁵, K. Nirunpong, A. Poll, S. Senkin, V.J. Smith, T. Williams

Rutherford Appleton Laboratory, Didcot, United Kingdom

L. Basso⁴⁹, K.W. Bell, A. Belyaev⁴⁹, C. Brew, R.M. Brown, D.J.A. Cockerill, J.A. Coughlan, K. Harder, S. Harper, J. Jackson, B.W. Kennedy, E. Olaiya, D. Petyt, B.C. Radburn-Smith, C.H. Shepherd-Themistocleous, I.R. Tomalin, W.J. Womersley

Imperial College, London, United Kingdom

R. Bainbridge, G. Ball, R. Beuselinck, O. Buchmuller, D. Colling, N. Cripps, M. Cutajar, P. Dauncey, G. Davies, M. Della Negra, W. Ferguson, J. Fulcher, D. Futyan, A. Gilbert, A. Guneratne Bryer, G. Hall, Z. Hatherell, J. Hays, G. Iles, M. Jarvis, G. Karapostoli, L. Lyons, A.-M. Magnan, J. Marrouche, B. Mathias, R. Nandi, J. Nash, A. Nikitenko³⁸, A. Papageorgiou, J. Pela, M. Pesaresi, K. Petridis, M. Pioppi⁵⁰, D.M. Raymond, S. Rogerson, A. Rose, M.J. Ryan, C. Seez, P. Sharp[†], A. Sparrow, M. Stoye, A. Tapper, M. Vazquez Acosta, T. Virdee, S. Wakefield, N. Wardle, T. Whyntie

Brunel University, Uxbridge, United Kingdom

M. Chadwick, J.E. Cole, P.R. Hobson, A. Khan, P. Kyberd, D. Leggat, D. Leslie, W. Martin, I.D. Reid, P. Symonds, L. Teodorescu, M. Turner

Baylor University, Waco, USA

K. Hatakeyama, H. Liu, T. Scarborough

The University of Alabama, Tuscaloosa, USA

O. Charaf, C. Henderson, P. Rumerio

Boston University, Boston, USA

A. Avetisyan, T. Bose, C. Fantasia, A. Heister, J. St. John, P. Lawson, D. Lazic, J. Rohlf, D. Sperka, L. Sulak

Brown University, Providence, USA

J. Alimena, S. Bhattacharya, D. Cutts, Z. Demiragli, A. Ferapontov, A. Garabedian, U. Heintz, S. Jabeen, G. Kukartsev, E. Laird, G. Landsberg, M. Luk, M. Narain, D. Nguyen, M. Segala, T. Sinthuprasith, T. Speer, K.V. Tsang

University of California, Davis, Davis, USA

R. Breedon, G. Breto, M. Calderon De La Barca Sanchez, S. Chauhan, M. Chertok, J. Conway, R. Conway, P.T. Cox, J. Dolen, R. Erbacher, M. Gardner, R. Houtz, W. Ko, A. Kopecky, R. Lander, O. Mall, T. Miceli, D. Pellett, F. Ricci-Tam, B. Rutherford, M. Searle, J. Smith, M. Squires, M. Tripathi, R. Vasquez Sierra, R. Yohay

University of California, Los Angeles, Los Angeles, USA

V. Andreev, D. Cline, R. Cousins, J. Duris, S. Erhan, P. Everaerts, C. Farrell, J. Hauser, M. Ignatenko, C. Jarvis, C. Plager, G. Rakness, P. Schlein[†], P. Traczyk, V. Valuev, M. Weber

University of California, Riverside, Riverside, USA

J. Babb, R. Clare, M.E. Dinardo, J. Ellison, J.W. Gary, F. Giordano, G. Hanson, G.Y. Jeng⁵¹, H. Liu, O.R. Long, A. Luthra, H. Nguyen, S. Paramesvaran, J. Sturdy, S. Sumowidagdo, R. Wilken, S. Wimpenny

University of California, San Diego, La Jolla, USA

W. Andrews, J.G. Branson, G.B. Cerati, S. Cittolin, D. Evans, F. Golf, A. Holzner, R. Kelley, M. Lebourgeois, J. Letts, I. Macneill, B. Mangano, S. Padhi, C. Palmer, G. Petrucciani, M. Pieri, M. Sani, V. Sharma, S. Simon, E. Sudano, M. Tadel, Y. Tu, A. Vartak, S. Wasserbaech⁵², F. Würthwein, A. Yagil, J. Yoo

University of California, Santa Barbara, Santa Barbara, USA

D. Barge, R. Bellan, C. Campagnari, M. D'Alfonso, T. Danielson, K. Flowers, P. Geffert, J. Incandela, C. Justus, P. Kalavase, S.A. Koay, D. Kovalskyi, V. Krutelyov, S. Lowette, N. Mccoll, V. Pavlunin, F. Rebassoo, J. Ribnik, J. Richman, R. Rossin, D. Stuart, W. To, C. West

California Institute of Technology, Pasadena, USA

A. Apresyan, A. Bornheim, Y. Chen, E. Di Marco, J. Duarte, M. Gataullin, Y. Ma, A. Mott, H.B. Newman, C. Rogan, M. Spiropulu, V. Timciuc, J. Veverka, R. Wilkinson, S. Xie, Y. Yang, R.Y. Zhu

Carnegie Mellon University, Pittsburgh, USA

B. Akgun, V. Azzolini, A. Calamba, R. Carroll, T. Ferguson, Y. Iiyama, D.W. Jang, Y.F. Liu, M. Paulini, H. Vogel, I. Vorobiev

University of Colorado at Boulder, Boulder, USA

J.P. Cumalat, B.R. Drell, W.T. Ford, A. Gaz, E. Luiggi Lopez, J.G. Smith, K. Stenson, K.A. Ulmer, S.R. Wagner

Cornell University, Ithaca, USA

J. Alexander, A. Chatterjee, N. Eggert, L.K. Gibbons, B. Heltsley, A. Khukhunaishvili, B. Kreis, N. Mirman, G. Nicolas Kaufman, J.R. Patterson, A. Ryd, E. Salvati, W. Sun, W.D. Teo, J. Thom, J. Thompson, J. Tucker, J. Vaughan, Y. Weng, L. Winstrom, P. Wittich

Fairfield University, Fairfield, USA

D. Winn

Fermi National Accelerator Laboratory, Batavia, USA

S. Abdullin, M. Albrow, J. Anderson, L.A.T. Bauerdick, A. Beretvas, J. Berryhill, P.C. Bhat, I. Bloch, K. Burkett, J.N. Butler, V. Chetluru, H.W.K. Cheung, F. Chlebana, V.D. Elvira, I. Fisk, J. Freeman, Y. Gao, D. Green, O. Gutsche, J. Hanlon, R.M. Harris, J. Hirschauer, B. Hooberman, S. Jindariani, M. Johnson, U. Joshi, B. Kilminster, B. Klima, S. Kunori, S. Kwan, C. Leonidopoulos, J. Linacre, D. Lincoln, R. Lipton, J. Lykken, K. Maeshima, J.M. Marraffino, S. Maruyama, D. Mason, P. McBride, K. Mishra, S. Mrenna, Y. Musienko⁵³, C. Newman-Holmes, V. O'Dell, O. Prokofyev, E. Sexton-Kennedy, S. Sharma, W.J. Spalding, L. Spiegel, L. Taylor, S. Tkaczyk, N.V. Tran, L. Uplegger, E.W. Vaandering, R. Vidal, J. Whitmore, W. Wu, F. Yang, F. Yumiceva, J.C. Yun

University of Florida, Gainesville, USA

D. Acosta, P. Avery, D. Bourilkov, M. Chen, T. Cheng, S. Das, M. De Gruttola, G.P. Di Giovanni, D. Dobur, A. Drozdetskiy, R.D. Field, M. Fisher, Y. Fu, I.K. Furic, J. Gartner, J. Hugon, B. Kim, J. Konigsberg, A. Korytov, A. Kropivnitskaya, T. Kypreos, J.F. Low, K. Matchev, P. Milenovic⁵⁴, G. Mitselmakher, L. Muniz, M. Park, R. Remington, A. Rinkevicius, P. Sellers, N. Skhirtladze, M. Snowball, J. Yelton, M. Zakaria

Florida International University, Miami, USA

V. Gaultney, S. Hewamanage, L.M. Lebolo, S. Linn, P. Markowitz, G. Martinez, J.L. Rodriguez

Florida State University, Tallahassee, USA

T. Adams, A. Askew, J. Bochenek, J. Chen, B. Diamond, S.V. Gleyzer, J. Haas, S. Hagopian, V. Hagopian, M. Jenkins, K.F. Johnson, H. Prosper, V. Veeraraghavan, M. Weinberg

Florida Institute of Technology, Melbourne, USA

M.M. Baarmann, B. Dorney, M. Hohlmann, H. Kalakhety, I. Vodopiyanov

University of Illinois at Chicago (UIC), Chicago, USA

M.R. Adams, I.M. Anghel, L. Apanasevich, Y. Bai, V.E. Bazterra, R.R. Betts, I. Bucinskaite, J. Callner, R. Cavanaugh, O. Evdokimov, L. Gauthier, C.E. Gerber, D.J. Hofman, S. Khalatyan, F. Lacroix, M. Malek, C. O'Brien, C. Silkworth, D. Strom, P. Turner, N. Varelas

The University of Iowa, Iowa City, USA

U. Akgun, E.A. Albayrak, B. Bilki⁵⁵, W. Clarida, F. Duru, J.-P. Merlo, H. Mermerkaya⁵⁶, A. Mestvirishvili, A. Moeller, J. Nachtman, C.R. Newsom, E. Norbeck, Y. Onel, F. Ozok⁵⁷, S. Sen, P. Tan, E. Tiras, J. Wetzel, T. Yetkin, K. Yi

Johns Hopkins University, Baltimore, USA

B.A. Barnett, B. Blumenfeld, S. Bolognesi, D. Fehling, G. Giurgiu, A.V. Gritsan, Z.J. Guo, G. Hu, P. Maksimovic, S. Rappoccio, M. Swartz, A. Whitbeck

The University of Kansas, Lawrence, USA

P. Baringer, A. Bean, G. Benelli, R.P. Kenny Iii, M. Murray, D. Noonan, S. Sanders, R. Stringer, G. Tinti, J.S. Wood, V. Zhukova

Kansas State University, Manhattan, USA

A.F. Barfuss, T. Bolton, I. Chakaberia, A. Ivanov, S. Khalil, M. Makouski, Y. Maravin, S. Shrestha, I. Svintradze

Lawrence Livermore National Laboratory, Livermore, USA

J. Gronberg, D. Lange, D. Wright

University of Maryland, College Park, USA

A. Baden, M. Boutemeur, B. Calvert, S.C. Eno, J.A. Gomez, N.J. Hadley, R.G. Kellogg, M. Kirn,

T. Kolberg, Y. Lu, M. Marionneau, A.C. Mignerey, K. Pedro, A. Skuja, J. Temple, M.B. Tonjes, S.C. Tonwar, E. Twedt

Massachusetts Institute of Technology, Cambridge, USA

A. Apyan, G. Bauer, J. Bendavid, W. Busza, E. Butz, I.A. Cali, M. Chan, V. Dutta, G. Gomez Ceballos, M. Goncharov, K.A. Hahn, Y. Kim, M. Klute, K. Krajczar⁵⁸, P.D. Luckey, T. Ma, S. Nahn, C. Paus, D. Ralph, C. Roland, G. Roland, M. Rudolph, G.S.F. Stephans, F. Stöckli, K. Sumorok, K. Sung, D. Velicanu, E.A. Wenger, R. Wolf, B. Wyslouch, M. Yang, Y. Yilmaz, A.S. Yoon, M. Zanetti

University of Minnesota, Minneapolis, USA

S.I. Cooper, B. Dahmes, A. De Benedetti, G. Franzoni, A. Gude, S.C. Kao, K. Klapoetke, Y. Kubota, J. Mans, N. Pastika, R. Rusack, M. Sasseville, A. Singovsky, N. Tambe, J. Turkewitz

University of Mississippi, Oxford, USA

L.M. Cremaldi, R. Kroeger, L. Perera, R. Rahmat, D.A. Sanders

University of Nebraska-Lincoln, Lincoln, USA

E. Avdeeva, K. Bloom, S. Bose, J. Butt, D.R. Claes, A. Dominguez, M. Eads, J. Keller, I. Kravchenko, J. Lazo-Flores, H. Malbouisson, S. Malik, G.R. Snow

State University of New York at Buffalo, Buffalo, USA

A. Godshalk, I. Iashvili, S. Jain, A. Kharchilava, A. Kumar

Northeastern University, Boston, USA

G. Alverson, E. Barberis, D. Baumgartel, M. Chasco, J. Haley, D. Nash, D. Trocino, D. Wood, J. Zhang

Northwestern University, Evanston, USA

A. Anastassov, A. Kubik, N. Mucia, N. Odell, R.A. Ofierzynski, B. Pollack, A. Pozdnyakov, M. Schmitt, S. Stoynev, M. Velasco, S. Won

University of Notre Dame, Notre Dame, USA

L. Antonelli, D. Berry, A. Brinkerhoff, K.M. Chan, M. Hildreth, C. Jessop, D.J. Karmgard, J. Kolb, K. Lannon, W. Luo, S. Lynch, N. Marinelli, D.M. Morse, T. Pearson, M. Planer, R. Ruchti, J. Slaunwhite, N. Valls, M. Wayne, M. Wolf

The Ohio State University, Columbus, USA

B. Bylsma, L.S. Durkin, C. Hill, R. Hughes, K. Kotov, T.Y. Ling, D. Puigh, M. Rodenburg, C. Vuosalo, G. Williams, B.L. Winer

Princeton University, Princeton, USA

N. Adam, E. Berry, P. Elmer, D. Gerbaudo, V. Halyo, P. Hebda, J. Hegeman, A. Hunt, P. Jindal, D. Lopes Pegna, P. Lujan, D. Marlow, T. Medvedeva, M. Mooney, J. Olsen, P. Piroué, X. Quan, A. Raval, B. Safdi, H. Saka, D. Stickland, C. Tully, J.S. Werner, A. Zuranski

University of Puerto Rico, Mayaguez, USA

E. Brownson, A. Lopez, H. Mendez, J.E. Ramirez Vargas

Purdue University, West Lafayette, USA

E. Alagoz, V.E. Barnes, D. Benedetti, G. Bolla, D. Bortoletto, M. De Mattia, A. Everett, Z. Hu, M. Jones, O. Koybasi, M. Kress, A.T. Laasanen, N. Leonardo, V. Maroussov, P. Merkel, D.H. Miller, N. Neumeister, I. Shipsey, D. Silvers, A. Svyatkovskiy, M. Vidal Marono, H.D. Yoo, J. Zablocki, Y. Zheng

Purdue University Calumet, Hammond, USA

S. Guragain, N. Parashar

Rice University, Houston, USA

A. Adair, C. Boulahouache, K.M. Ecklund, F.J.M. Geurts, W. Li, B.P. Padley, R. Redjimi, J. Roberts, J. Zabel

University of Rochester, Rochester, USA

B. Betchart, A. Bodek, Y.S. Chung, R. Covarelli, P. de Barbaro, R. Demina, Y. Eshaq, T. Ferbel, A. Garcia-Bellido, P. Goldenzweig, J. Han, A. Harel, D.C. Miner, D. Vishnevskiy, M. Zielinski

The Rockefeller University, New York, USA

A. Bhatti, R. Ciesielski, L. Demortier, K. Goulianatos, G. Lungu, S. Malik, C. Mesropian

Rutgers, the State University of New Jersey, Piscataway, USA

S. Arora, A. Barker, J.P. Chou, C. Contreras-Campana, E. Contreras-Campana, D. Duggan, D. Ferencek, Y. Gershtein, R. Gray, E. Halkiadakis, D. Hidas, A. Lath, S. Panwalkar, M. Park, R. Patel, V. Rekovic, J. Robles, K. Rose, S. Salur, S. Schnetzer, C. Seitz, S. Somalwar, R. Stone, S. Thomas

University of Tennessee, Knoxville, USA

G. Cerizza, M. Hollingsworth, S. Spanier, Z.C. Yang, A. York

Texas A&M University, College Station, USA

R. Eusebi, W. Flanagan, J. Gilmore, T. Kamon⁵⁹, V. Khotilovich, R. Montalvo, I. Osipenkov, Y. Pakhotin, A. Perloff, J. Roe, A. Safonov, T. Sakuma, S. Sengupta, I. Suarez, A. Tatarinov, D. Toback

Texas Tech University, Lubbock, USA

N. Akchurin, J. Damgov, C. Dragoiu, P.R. Dudero, C. Jeong, K. Kovitanggoon, S.W. Lee, T. Libeiro, Y. Roh, I. Volobouev

Vanderbilt University, Nashville, USA

E. Appelt, A.G. Delannoy, C. Florez, S. Greene, A. Gurrola, W. Johns, P. Kurt, C. Maguire, A. Melo, M. Sharma, P. Sheldon, B. Snook, S. Tuo, J. Velkovska

University of Virginia, Charlottesville, USA

M.W. Arenton, M. Balazs, S. Boutle, B. Cox, B. Francis, J. Goodell, R. Hirosky, A. Ledovskoy, C. Lin, C. Neu, J. Wood

Wayne State University, Detroit, USA

S. Gollapinni, R. Harr, P.E. Karchin, C. Kottachchi Kankamamge Don, P. Lamichhane, A. Sakharov

University of Wisconsin, Madison, USA

M. Anderson, D. Belknap, L. Borrello, D. Carlsmith, M. Cepeda, S. Dasu, E. Friis, L. Gray, K.S. Grogg, M. Grothe, R. Hall-Wilton, M. Herndon, A. Hervé, P. Klabbers, J. Klukas, A. Lanaro, C. Lazaridis, J. Leonard, R. Loveless, A. Mohapatra, I. Ojalvo, F. Palmonari, G.A. Pierro, I. Ross, A. Savin, W.H. Smith, J. Swanson

†: Deceased

1: Also at Vienna University of Technology, Vienna, Austria

2: Also at National Institute of Chemical Physics and Biophysics, Tallinn, Estonia

3: Also at Universidade Federal do ABC, Santo Andre, Brazil

4: Also at California Institute of Technology, Pasadena, USA

- 5: Also at CERN, European Organization for Nuclear Research, Geneva, Switzerland
- 6: Also at Laboratoire Leprince-Ringuet, Ecole Polytechnique, IN2P3-CNRS, Palaiseau, France
- 7: Also at Suez Canal University, Suez, Egypt
- 8: Also at Zewail City of Science and Technology, Zewail, Egypt
- 9: Also at Cairo University, Cairo, Egypt
- 10: Also at Fayoum University, El-Fayoum, Egypt
- 11: Also at British University in Egypt, Cairo, Egypt
- 12: Now at Ain Shams University, Cairo, Egypt
- 13: Also at National Centre for Nuclear Research, Swierk, Poland
- 14: Also at Université de Haute-Alsace, Mulhouse, France
- 15: Now at Joint Institute for Nuclear Research, Dubna, Russia
- 16: Also at Moscow State University, Moscow, Russia
- 17: Also at Brandenburg University of Technology, Cottbus, Germany
- 18: Also at Institute of Nuclear Research ATOMKI, Debrecen, Hungary
- 19: Also at Eötvös Loránd University, Budapest, Hungary
- 20: Also at Tata Institute of Fundamental Research - HECR, Mumbai, India
- 21: Also at University of Visva-Bharati, Santiniketan, India
- 22: Also at Sharif University of Technology, Tehran, Iran
- 23: Also at Isfahan University of Technology, Isfahan, Iran
- 24: Also at Plasma Physics Research Center, Science and Research Branch, Islamic Azad University, Tehran, Iran
- 25: Also at Facoltà Ingegneria, Università di Roma, Roma, Italy
- 26: Also at Università della Basilicata, Potenza, Italy
- 27: Also at Università degli Studi Guglielmo Marconi, Roma, Italy
- 28: Also at Università degli Studi di Siena, Siena, Italy
- 29: Also at University of Bucharest, Faculty of Physics, Bucuresti-Magurele, Romania
- 30: Also at Faculty of Physics of University of Belgrade, Belgrade, Serbia
- 31: Also at University of California, Los Angeles, Los Angeles, USA
- 32: Also at Scuola Normale e Sezione dell'INFN, Pisa, Italy
- 33: Also at INFN Sezione di Roma; Università di Roma, Roma, Italy
- 34: Also at University of Athens, Athens, Greece
- 35: Also at Rutherford Appleton Laboratory, Didcot, United Kingdom
- 36: Also at The University of Kansas, Lawrence, USA
- 37: Also at Paul Scherrer Institut, Villigen, Switzerland
- 38: Also at Institute for Theoretical and Experimental Physics, Moscow, Russia
- 39: Also at Albert Einstein Center for Fundamental Physics, Bern, Switzerland
- 40: Also at Gaziosmanpasa University, Tokat, Turkey
- 41: Also at Adiyaman University, Adiyaman, Turkey
- 42: Also at Izmir Institute of Technology, Izmir, Turkey
- 43: Also at The University of Iowa, Iowa City, USA
- 44: Also at Mersin University, Mersin, Turkey
- 45: Also at Ozyegin University, Istanbul, Turkey
- 46: Also at Kafkas University, Kars, Turkey
- 47: Also at Suleyman Demirel University, Isparta, Turkey
- 48: Also at Ege University, Izmir, Turkey
- 49: Also at School of Physics and Astronomy, University of Southampton, Southampton, United Kingdom
- 50: Also at INFN Sezione di Perugia; Università di Perugia, Perugia, Italy
- 51: Also at University of Sydney, Sydney, Australia

- 52: Also at Utah Valley University, Orem, USA
- 53: Also at Institute for Nuclear Research, Moscow, Russia
- 54: Also at University of Belgrade, Faculty of Physics and Vinca Institute of Nuclear Sciences, Belgrade, Serbia
- 55: Also at Argonne National Laboratory, Argonne, USA
- 56: Also at Erzincan University, Erzincan, Turkey
- 57: Also at Mimar Sinan University, Istanbul, Istanbul, Turkey
- 58: Also at KFKI Research Institute for Particle and Nuclear Physics, Budapest, Hungary
- 59: Also at Kyungpook National University, Daegu, Korea